AD-A067 091   NAVAL RESEARCH LAB   WASHINGTON D C   F/G 9/3
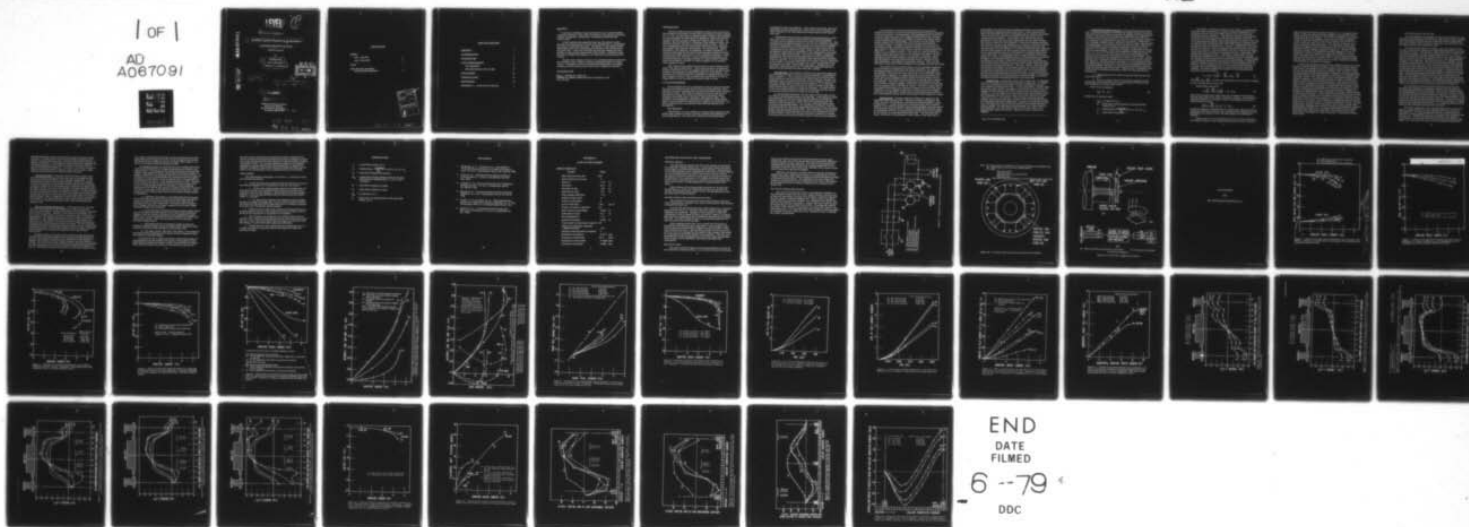   TRANSIENT CHARACTERISTICS OF DC MACHINERY TRANSIENT BEHAVIOR OF--ETC(U)
                AUG 52   J CYBULSKI, J P O'CONNOR, E L BRANCATO

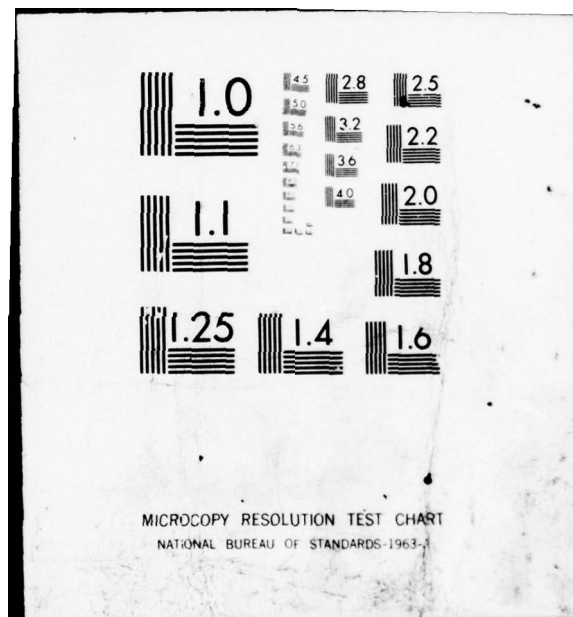UNCLASSIFIED   NRL-MR-63   NL

| OF |
AD
A067091

MICROCOPY RESOLUTION TEST CHART

NATIONAL BUREAU OF STANDARDS-1963-A

LEVEL

C

NRL Memorandum Report 63 (U)

TRANSIENT CHARACTERISTICS OF DC MACHINERY

TRANSIENT BEHAVIOR OF FLUX

(Interim Report)

by

John Cybulski,
John P. O'Connor
Emanuel L. Brancato

49 p.

NRL-MR-63

25 August 1952

Shipboard Systems Branch
Electricity Division
Naval Research Laboratory
Washington 25, D.C. DC 20375

251 950

79 04 06 022

DISTRIBUTION

BuShips

    Attn: Code 560   1

    Attn: Code 560U   6

BuAer   1

CDR Material Laboratory
   New York Naval Shipyard   2

TABLE OF CONTENTS

ABSTRACT

Accurate calculation of the current flow in a d-c machine during a transient requires a study of the flux behavior which governs generated voltage, leakage flux, commutation, coefficients of induction and eddy-current.

It was found that the magnitude of air-gap flux suffers a small decrease up to peak transient current while its distortion is considerable and effects commutation adversely. The quality of commutation further deteriorates with vicious sparking and arcing due to the slow growth of interpolar flux. It was also noted that the main-pole leakage flux does not keep in step with the induced shunt field current. Application of the theorem of constant flux linkages is in small error up to peak armature current.

Blocked rotor testing is found to be a practical method to determine flux variations under transient conditions approaching those of a short circuit. Techniques for flux measurements during static and rotating conditions and the measurement of bar-to-bar voltages are outlined.

AUTHORIZATION

1.

INTRODUCTION

Previous studies (1) have stressed the need for more accuracy in the calculation of transient currents than is provided by present methods (2, 3, 4, 5). For the design of shipboard power systems, these methods are not sufficiently accurate and do not adequately reflect the influence of initial conditions of load, voltage, and speed on peak currents. In addition, they are deficient in predicting, within design accuracy, the build-up and decay of armature and field circuit currents. There is also a disappointing lack of experimental verification of the important assumptions upon which the theoreticians were proceeding. Before developing a new approach, or following a published calculation, it becomes evident that the limitations of the proposed relations are determined by the validity and accuracy of the assumption employed. It was concluded from this work that a more fundamental knowledge of the internal phenomena of rotating machinery is required before relations may be formulated to calculate transient response of a dc machine within design accuracy.

This report on flux behavior is the first of a series devoted to the study of the internal phenomena. Flux is given primary consideration because it governs the over-all magnetic behavior of the machine in that it dictates the magnitude of generated voltage and of inductances. By alteration of its path it affects the coefficient of coupling between two or more magnetic circuits, such as shunt field and armature; its rate of change affects circuit resistance by means of eddy currents.

FLUX MEASUREMENTS

The air-gap flux has as its components the direct-axis flux through the main pole produced by the shunt- and series-field windings, and a quadrature axis flux resulting from the mmf of the difference of armature and interpole mmf. Both of these components of the air-gap flux are affected by the leakage flux of the main poles and interpoles, and by saturation of the main poles, interpoles, and armature teeth. Flux variations causing changes in the generated voltage can manifest themselves in one or both of two ways: (a) by a change in flux magnitude, and (b) by a distortion due to an effective shift in the distribution of the air-gap flux.

Flux Magnitude

Unfortunately, it is very difficult to measure the air-gap flux under steady-state conditions without resorting to special and elaborate features. (Appendix A). The imposition of short-circuits makes these

arrangements even more difficult. It was found, fortunately, that much useful data could be obtained easily under blocked rotor conditions and that correlation of this information with normal short-circuit tests is quite good.

The blocked rotor procedure eliminated the high-frequency variation in flux due to armature slots and thus permitted oscillographic recording of flux changes by means of the probe coils (Appendix A). This technique was considered satisfactory since the flux variations sought are essentially independent of machine rotation except for those variations caused by effective brush shift resulting from a change in the point of commutation and the effects of arcing. However, these effects can be simulated to some extent by shifting the brush rigging and by increasing the effective width of the brushes. The former condition emphasized commutation shift while the latter approaches the arcing phenomenon. Blocked rotor tests were first utilized in determination of the magnitude of the air-gap flux. In the presentation of flux data, fluxes are expressed in per unit (p.u.) quantities and employ for a base the magnitude of the air-gap flux at no load, rated voltage, and speed. Leakage flux of the main pole, expressed in per unit, is obtained by taking the difference between the core and the main-pole shoe-flux readings.

Air-Gap Flux. The transient variation of air-gap and leakage flux as a function of armature current for several degrees of compounding is shown in Figure 1. The two factors that determine the characteristics observed here are the series field mmf, which influences, directly, the magnitude of the air-gap flux and the direct-axis component of the armature mmf, which tends to decrease the air-gap flux. In a cumulative compound machine the two factors tend to cancel, whereas in the differential machine they combine to reduce the total flux. The effectiveness of the series field during these conditions is dependent upon the number of turns and location of the coil relative to the air gap.

As will be indicated shortly, the time taken to reach peak current is a factor in determining the loss of air-gap flux. In an attempt to check this hypothesis, the flux loss (Figure 2) was obtained at 0.08 second (time for armature current to reach 95% of peak magnitude) after the initiation of the transient for a series of tests, where the steady-state current is progressively higher. In a comparison of Figures 1 and 2 it is found that the flux loss at any magnitude of armature current is proportional to the time to attain that current. This observation is corroborated by data obtained during actual short circuits on the machine and is presented in Figure 3 where the main-pole shoe-flux is plotted as a function of armature circuit current for several values of short-circuit resistance.

3.

It was pointed out earlier that the blocked rotor tests did not simulate the effective brush shift normally encountered during a transient. As the test machine is a differentially compounded generator, tests were made by shifting the entire brush rigging mechanically in the direction of rotation under blocked rotor conditions to produce the effects similar to that of differential compounding. This results from the larger component of direct-axis armature reaction above that encountered for on-neutral setting. A comparison of the reduction of air-gap flux for brush shift of three commutator segments with that for the neutral position, Figure 4, shows an increase in flux reduction of approximately 100 - 200% at 3 p.u. armature current. This, however, does not produce a totally accurate picture of flux loss, for brush arcing reflects not only a shifting of the commutation point in the direction of rotation, which introduces a direct-axis component of armature reaction, but reduces also the effective coil sides due to shorting of turns. The loss in coil sides diminishes the magnitude of armature reaction. Thus, the flux decrease is less severe under conditions of arcing than of brush shift alone.

To simulate arcing conditions better, three commutator segments (in the direction of rotation) were effectively shorted to the segments normally spanned by the brushes for each of the four brush holders of the machine. Because an arc does not provide a zero resistance "short" of commutator segments, it is expected that the actual loss of flux will follow some curve between boundary characteristics dictated by brush shift only and by the effective brush shift due to shorting of the commutator segments. The effect of this arrangement on the transient air-gap flux is shown in Figure 5 together with the flux variation for a brush shift of three segments and for brushes on neutral. The flux in steady state is also shown on this figure as a function of armature current for the same conditions of brush rigging by which the transient trials were obtained. Reduction in air-gap flux in steady state is considerably greater than for the corresponding transient trials; the passage of time is again the reason.

Interpole Flux. Of equal importance with the air-gap flux is the magnitude of the interpole flux. The actual behavior of magnetic flux within and below the interpole is important for understanding the commutating process. A major portion of a prevailing theory (3) of transient behavior of dc machines depends upon assumed negligible interpole effects which permits large increase in reactance voltage which shifts the point of commutation (current reversal) towards the edge of the brush allowing for completion of commutation below the brush. The interpolar pole pieces are placed in the quadrature (with respect to the main pole or

4.

direct field) axis with the interpole winding connected so as to oppose
the quadrature component of the armature mmf. Under blocked rotor
test it was found that the type of compounding did not influence the growth
of flux in the core or shoe of the interpole, thus the curves for all
connections were identical. It was noted, also, that the increase in
interpole core flux was practically independent of brush shift, whereas
the increase of shoe flux was dependent. Plots of the transient interpole
shoe and core flux are seen in Figure 6 as a function of armature current.
The curve for the three-segment brush shift represents the core flux
characteristics for all brush positions between neutral and three segments.
The shoe flux growth for the three-segment shift is greater than that for
the on-neutral position because of the decrease in demagnetization mmf
in the direct axis. Corresponding to the air-gap flux short circuit data
(Figure 3), curves illustrating the build-up of interpole flux are presented
in Figure 7 as a function of the transient armature circuit current.
Examination of this figure reveals an initial penetration of the interpole
face by flux from the armature conductors which means additional voltage
is generated opposing commutation. This flux, however, does not reach
the interpole core region in any sizable quantity, due to the increasing
effectiveness of interpole mmf and to growth of eddy currents within the
interpole preventing penetration of the entire pole. It is surmised that
the closeness of the interpole and main pole shoes permits a considerable
leakage of interpole flux to the shunt pole structure tending to accentuate
the magnetizing and demangetizing action on the main pole.

Leakage Flux. During these same short-circuit runs, oscillograph
records were made of the transient shunt-pole leakage flux. A compari-
son can be made between the results of these runs (Figure 8) and the
curve obtained during blocked rotor. It can be noted there, that the higher
the short-circuit current, the greater the deviation of the increase of
leakage flux with induced shunt field current from the theoretical linear
relation.[+] It is also apparent that the blocked rotor test simulated condi-
tions adequately up to the lowest short-circuit trial wherein the peak
current of 5.5 p.u. was reached. This deviation from the proposed
relation could be due to the effect of eddy-current in the yoke preventing
the immediate build-up of leakage flux. In order to evaluate this discrep-
ancy, the difference between the experimental value and the theoretical
value of leakage was expressed as a percentage error with respect to
the theoretical. For the series of short-circuit runs, this error is
approximately 25% at 0.02 second - the time for peak current to be
attained.

[+] Eq. 27 of reference (3).

5.

Constant Flux Linkage Theorem. In the study of transient proper-
ties of rotating machines the Constant Flux Linkage Theorem becomes a
very useful tool to calculate the increase in leakage flux during transient
loading, in the light of the knowledge that leakage flux increases as a
function of field current increase (c.f. fig. 8). It is important, therefore,
to re-examine its applicability as well as its limitation. Using Ohm's
Law, Faraday's Induction Law, and Lenz's Law as a basis, one can write
the fundamental circuit equations about electrical circuits. When there
is a discontinuity in action (closing or opening a switch), there are
theorems, for example, conservation of energy, conservation of charge,
and constant flux linkage, which can be applied to bridge the gap in time
from $t = o^-$ to $t = o^+$. Of major importance to flux variations is the
application of the theorem concerning constancy of flux linkages. This
theorem states that if the resistance of a closed circuit is zero, then the
algebraic sum of magnetic linkages of the circuit must remain constant
(6). However, whenever there is resistance, as in any practical circuit,
and elapsed time to contend with, there will be some deviation from the
initial flux linkages; therefore, it is desirable to establish a range over
which this theorem may be held valid. This theorem is employed in con-
junction with the following assumptions which are made generally for
convenience.

a. Leakage flux and the useful air-gap flux links all the turns
of the shunt field.

b. There is a linear build-up of shunt pole leakage flux with
the induced rise of shunt field current proportional to the ratio of the
initial leakage to the initial field current.

Under these assumptions

$$\phi_{ag} = \phi_c - n_f i_f \tag{1}$$

defines the air-gap flux where

ϕ_{ag} = air-gap flux in p.u.

ϕ_c = shunt-pole core-flux (junction of main pole with frame) in p.u.

n_f = leakage factor $(\frac{\phi \text{ leakage}}{\phi_{ag}})$ in p.u. at 1 p.u. i_f

i_f = shunt field current in p.u.

6.

In an effort to evaluate the utility of this relation, a measurement was made of the air-gap flux in a series of transient loadings of 5 p.u. armature current at the same initial field current, but for various shunt-field circuit resistance. The transient variation of air-gap flux for three values of field circuit resistance are plotted in Figure 9. From these curves it appears that for the same current (time is the same as the transients were all the same magnitude) there is a greater loss of air-gap flux and a resulting greater loss of flux linkages the larger the resistance in the shunt field circuit. However, with decrease in air-gap flux there is also an increase of leakage flux while the field current increases by induction. Since the field current rise is least for the higher shunt-field circuit resistance, the leakage flux and, consequently, the leakage flux linkages are least. This means, qualitatively, that the greater the resistance in the circuit, the greater the loss of linkages, as was expected from the theorem of constant flux linkages. As the problem of evaluating the magnitude of any partial leakage linkages is difficult, a simpler method was resorted to in order to evaluate quantitatively the difference in flux linkage loss for the various resistances and also to ascertain the the flux linkage loss as a percentage of the initial flux linkages. An ordinary differential equation can be written about the shunt field circuit as follows:

$$V_f = R_f i_f + L_f \frac{di_f}{dt} + \sum_n M_{fn} \frac{di_n}{dt} \tag{2}$$

where $\sum_n M_{fn} \frac{di_n}{dt}$ includes the mutual effects of all the other windings having coupling with the shunt field.

Rearranging equation (2)

$$L_f \frac{di_f}{dt} + \sum_n M_{fn} \frac{di_n}{dt} = V_f - R_f i_f \tag{3}$$

where the left-hand terms express the rate of change of flux linkages with the shunt field circuit when L and M are constant. A more general expression allows for a variable L and M so that Equation (3) can be reformulated as follows:

$$\frac{d}{dt}(L_f i_f + \sum_n M_n i_n) = V_f - R_f i_f \tag{4}$$

It therefore appears reasonable that by evaluating the right-hand side of Equation (4) one determines the rate of change of flux linkages; and upon integration with respect to time, the total change of flux linkages is obtained.

Equation (4) was first evaluated on the series of trials where the shunt field resistances were changed (discussed previously in relation to

7.

Figure 9) with the results as plotted in Figure 10. It is apparent from Figure 10 that a greater loss of flux linkages occurs with the larger circuit resistance, but that the over-all loss of linkages is quite small compared to the initial linkages. Since the rate of rise of armature circuit current was small for this type of blocked rotor transient, a similar study was made on the loss of flux linkages during the set of short-circuit tests mentioned before. For the series of four tests reported in Figures 3 and 8 a calculation on the loss of flux linkages was made and the results are plotted in Figure 11. The loss of flux linkages is greater for the greatest transient although the over-all magnitude is small in comparison to the initial linkages. In these trials, the maximum loss of flux linkages at peak armature current was about 5% for a zero resistance fault. A rate of change of linkages with the shunt field is the reason for an increase of shunt field current in the attempt at maintenance of linkages.

Mention has already been made of the change in shunt field current during a transient change of armature current, of the relation between field current and leakage flux, and of the part played by leakage flux in the over-all determination of the air-gap flux. The variation in field current results from the rapid change in armature-circuit demagnetizing mmf which induces in the field winding a current that is a function of the armature current. The relationship of this incremental change in field current to armature current during transient variation in the latter is shown in Figure 12 for the blocked rotor trials. The increase in shunt field current is greatest for the differentially compounded machine and least for the cumulative connection. Furthermore, the increase of field current is greater with brush shift in the direction of rotation for each quality of compounding than that for the neutral position, owing to the presence of a greater direct-axis component of armature reaction tending to reduce the air-gap flux. For the set of the aforementioned short-circuit trials a number of points for each condition depicting incremental rise of shunt field current are shown in Figure 13 as a function of the incremental armature circuit current. This illustrates a significant linearity between shunt field current and armature current up to peak field current. Included in this figure are plots of the incremental rise of field current under blocked rotor conditions with brushes on neutral and shifted three segments (abstracted from Figure 12). A comparison between the short-circuit and blocked rotor data affords some idea of the effective brush shift from neutral resulting from a shift in the point of commutation during a short circuit.

8.

Flux Distribution in the Air-Gap

Up to this point the investigation has dealt in part with the air-gap flux and revealed the change in total flux as affected by armature reaction. The distribution of this air-gap flux is significant since it determines bar-to-bar voltage, affects armature inductance, and determines inter-pole effectiveness in the commutation zone.

To obtain some preliminary results, coils were inserted in the air-gap to measure the change in the steady-state distribution as caused by armature current. The changes in distribution of the air-gap flux as a function of armature winding current (steps of 0.5, 1.0, 1.5 p.u.) with no shunt field or interpole winding excitation are shown in Figure 14. With only initial shunt field excitation of 1.5 p.u. the results indicated in Figure 15 are obtained. This shunt field excitation produces some saturation of the main poles which in turn lessens the change in the distribution below the main pole. The interpoles, however, are affected little by the shunt field although they are observed (Figures 14 and 15) to saturate as the armature current is increased. In contrast, the region beneath the center of the main pole exhibits no apparent saturation and an almost linear change of flux with distance up to the bevel on the shoe. The nonlinearity beyond this point is due to saturation of the main pole tips and the variation in air-gap length at the end of the main pole shoe and beneath the interpole. By adding the changes indicated in Figure 15 to the initial distribution due to the shunt field excitation, one obtains the complete air-gap distribution illustrated in Figure 16.

An indication of the air-gap flux distribution during transient excitation was acquired by recording the signals of the air-gap coils oscillographically and then integrating. The coils were mounted in the air-gap (Appendix A) for approximately one pole pitch with the assumption that all pole-pitch flux distributions are identical. In Figure 17 may be seen the transient air-gap flux distribution for a differentially connect-ed machine with the interpole windings connected. A comparison can be made of the air-gap flux distribution at various times during a test pulse with the initial air-gap flux distribution. It is noted that the flux neutral shifts quickly during the early part of the transient.

The effect of interpoles on air-gap flux distribution can be evalu-ated by comparing Figure 17, where the interpoles were energized, with Figure 18. It is observed that the build-up of interpole mmf is effective in limiting quickly the amount of armature flux coming into the interpole face. Besides affecting the air-gap flux in the region of commutation, the interpoles also influence the flux distribution at both edges of the main pole to the extent of accentuating the magnetization

9.

and demagnetization action of the armature conductors upon the main pole face. A similar set of curves for cumulative connection of the machine with and without interpole winding is illustrated in Figures 19 and 20, respectively. From Figures 17 and 19, the net air-gap flux was calculated and plotted as a function of armature current for the two machine connections in Figure 21. In essence, the result is similar to those presented previously in Figures 1 and 3; there is only a small change in air-gap flux for the very short times involved.

Flux Neutral Shift. It has been shown that there is only a very small net change of air-gap flux for some time, even though the flux neutral and the distribution have been changed considerably. A plot illustrating the amount of flux neutral shift as a function of armature current with machine connected differentially with interpole excitation is shown in Figure 22 for two blocked rotor transients. It appears that the higher the rate of rise of current (higher transient) the more linear the shift of neutral with respect to armature current. In Figure 22 there is also plotted the flux neutral shift which was found from a steady-state distribution when the machine was connected simple shunt and no interpole excitation. When a comparison is made of the curves in this figure there appears to be some time lag in neutral shift with the transient current, but no immediate saturation in the shift as exhibited by the transient tests.

Bar-to-bar Voltage Distribution. If the pattern of the transient flux distributions had been made available for study during actual short-circuit conditions, the generated voltage of the machine could have been examined in detail. However, since this was not feasible, the bar-to-bar voltages along an auxiliary commutator were recorded oscillographically. (A complete discussion of this procedure is outlined in Appendix A.) The voltage drops with the auxiliary commutator were taken over one pole pitch; it is assumed that this voltage distribution is representative of that beneath the other main poles. If it were possible to add the resistance and inductive drops to each bar-to-bar voltage drop, a distribution curve would be obtained which would accurately represent the flux distribution or generated voltage in the air gap during a short circuit.

During two short-circuit tests the bar-to-bar voltage distribution was found for initial load conditions of no load and full load (Figures 23 and 24). These plots are similar to the transient flux distribution for blocked rotor condition with and without interpole connection (Figures 17 and 18). The bar-to-bar curves in Figures 23 and 24 could be represented by a flux distribution between the two extremes indicated in Figures 17 and 18. This follows because during a short circuit the interpole current

10.

is, in effect, diverted thus reducing the interpole effectiveness to the extent illustrated by Figure 23 or 24. These two figures also indicate that the bar-to-bar voltage neutral (zero voltage) shifts rapidly -- as quickly as the flux neutral discussed previously.

An integration of the curves of the bar-to-bar voltage distribution can be made which results in a voltage distribution with respect to the negative brush. One example of the voltage distribution computed with respect to the negative brush for various times during the transient is plotted in Figure 25 corresponding to the bar-to-bar curves of Figure 23. In Figure 25 it may be observed that the potential between the negative and positive brush holders, at the commutator level, is approximately 72 volts after 0.02 second -- time to peak armature current. However, the air-gap flux for this run and at this time is shown in Figure 3 as 0.78 p.u. which would provide 170 volts under no load conditions. Subtraction of 36 volts for the armature resistance drop from 170 leaves 134 volts, or an excess of 62 volts over the 72 volts measured. This presents an interesting problem with several possible reasons offered in explanation:

a. Although commutation is completed within the brush span, reversal of flux around each coil side may not have been concluded because of the inherent lag in the change of flux with respect the the excitation mmf in an iron-clad circuit. Any further rate of change in these linkages will induce a voltage in opposition to the active useful generated voltage thus reducing it.

b. As the armature current grows the resultant magnetomotive force of the shunt field and armature circuit shifts in the direction of rotation. With the resultant distribution of flux lagging the magnetomotive force, it is then possible that at peak armature current the flux shifts still continues. This continued shift serves to reduce the generated voltage further.

c. During the period of commutation of high currents the armature winding exhibits a virtual resistance higher than the dc ohmic resistance because of reflected effects from the iron core.

d. This short circuit, like most of the others, is accompanied by flashing on the commutator to the extent of several segments which may reduce the terminal voltage.

It can also be seen in Figure 25 that the voltage neutral (point of zero potential on the commutator with respect to the negative brush) shifts quickly along the commutator surface in the direction of rotation. From what has already been said it is expected that the greater the

11.

the short circuit, the greater the progressive shift of voltage will be. This is confirmed for the group of short-circuit tests in Figure 26 where the voltage distributions have been plotted at 0.005 second after initiation of the short circuit. The results presented in Figures 23 through 26, although not representing the actual flux distribution, do indicate the algebraic summation of generated voltage and;impedance drops which is useful in the interpretation of the arcing phenomenon at the brushes.

CONCLUSIONS

The experimental investigation on a 90-hp d.c. machine has led to the following conclusions.

1. It was found that the air-gap flux does not decrease as much as was expected (Equation (1)) during short circuit for two reasons:

a. Steady-state proportionality between the leakage flux and shunt field current is not maintained during short circuit due to eddy-currents in the yoke and saturation. The assumption of proportionality would be in error by approximately 25% if it were used for the subject 90-hp d.c. machine.

b. As regards the relating of the change in leakage linkages directly to a change in leakage flux, it can be shown that the assumption that shunt field flux links all the shunt field turns is a dubious procedure since there are considerable partial linkages.

2. Whenever use is made of the constant flux linkage theorem up to peak armature current, it may entrail an error of as much as 5% for the 90-hp test machine due to an actual loss of linkages.

3. The interpoles are ineffective in providing sufficient flux to counteract the reactance voltage generated in the coils being commutated. They do, in fact, allow flux to build-up in that region in a direction such that voltages are generated further opposing commutation.

4. Results that have been obtained thus far indicate that there is a large unaccounted for potential drop at the brushes and within the armature winding.

12.

NOMENCLATURE

i_f = shunt field current; in p.u.

n_f = leakage factor $\left(\dfrac{\phi \text{ leakage}}{\phi_{ag}}\right)$; in p.u. at 1 p.u. i_f.

L_f = shunt field inductance; in henries.

M_{fn} = coefficient of mutual induction between the shunt field and other windings with $n = 1, 2, 3$, etc.; in henries.

R_f = shunt field resistance; in ohms.

V_f = shunt field excitation; in volts.

ϕ_{ag} = air gap flux; in p.u.

ϕ_c = shunt-pole core flux (junction of main pole with frame); in p.u.

REFERENCES

1. McClinton, A. T., Brancato, E. L., and Panoff, R.
   "Transient Characteristics of D-C Motors and Genera-
   tors", A.I.E.E. Transactions, Part II, 68; 1100-06, 1949.

2. Frost, G. E., "The Short-Circuit Characteristics of
   D-C Generators", A.I.E.E. Transactions, 65; 394-
   402, 1946.

3. Linville, T. M., "Current and Torque of D-C Machines
   On Short-Circuit", A.I.E.E. Transactions, Part I,
   69, 956-65, 1946.

4. Koenig, H. E., "Transient Response of Direct-Current
   Dynamos", A.I.E.E. Transactions, Part I, 69; 139-45,
   1950.

5. Vowels, R. E. and Forte, W. G., "Electromechanical
   Analysis of a Separately Excited D-C Machine", A.I.E.E.
   Transactions, Part I, 71: Technical Paper 52-45, 1952.

6. Doherty, R. E., "A Simplified Method of Analyzing
   Short-Circuit Problems," A.I.E.E. Transactions, 52:
   841, 1923.

APPENDIX A

90-HP DC TEST MACHINE

DESIGN CONSTANTS

Quantity	Value	
Shunt field turns per pole	2100	
Series field turns per pole	2	
Pole arc	7.77	in.
Pole pitch	10.8	in.
Interpole air gap	1/16	in.
Main-pole air gap	1/8	in.
Field leakage coefficient	1.12	
Number of main poles	4	
Number of interpoles	4	
Area of field poles	28.7	sq. in.
Number of armture conductors	170	
Mean section of tooth width	0.598	in.
Axial depth of tooth	0.3	in.
Slot fringing factor	1.12	
Armature slot pitch	0.996	in.
Total number of commutator segments	85	
Number of commutator segments spanned by brush	1.64	
Number of parallel paths in armature	2	
Resistance of armature	0.0141	ohm
Resistance of shunt field	36.8	ohms
Resistance of series field	0.00168	ohm
Resistance of interpole	0.0045	ohm

METHODS AND DETAILS OF TEST PROCEDURE

Schematic Diagram

The experimental setup for the 90-hp test machine is illustrated by a schematic diagram (Figure A1). A synchronous switch (not shown in this figure) controlled automatically and in sequence: (a) starting of the oscillograph paper drive, (b) initiation of the short circuit by tripping of a spring-loaded single-pole knife switch which connects various amounts of resistance in the form of iron grids across the terminals of the machine (run as a generator), (c) tripping of the 2600-ampere air breaker after a specified time of 0.2 second to prevent excessive damage to the machines, and (d) stopping the oscillograph paper drive motor.

Other features of this setup include provision to: (a) drive the test machine as a motor, (b) loading the machine in pump back, (c) load the test machine before a short circuit, and (d) separately excite the shunt fields of both machines.

Location of Probe Coils and Measurement of Flux

The location of the probe coils at the main pole shoe, main pole core, interpole shoe, interpole core, and the yoke (frame) of the machine is sketched in Figure A2.

To obtain the total integrated value of flux change over a relatively long period of time (2 to 3 seconds) a Sensitive Research Multirange Fluxmeter was employed. Whenever it was desirable to obtain the instantaneous rates of change of flux in the various regions, a magnetic galvanometer oscillograph of The Consolidated Engineering Corporation was used. The total changes of flux were integrated graphically over short periods of time (0.002 second).

Twelve adjacent probe coils used to obtain the distribution of air-gap flux were placed in the air gap within a region slightly larger than one pole pitch and extending in depth from the commutator risers to the armature end turns. The mechanical problem of mounting these coils so as not to be damaged by the rotation of the armature was solved by conducting the tests under blocked rotor conditions. This also eliminated the hash in the flux signals due to both tooth ripple and sparking at the brushes, and the difficulties and effects associated with commutation.

Block Rotor Tests

The setup outlined in Figure A1 included provision for driving the test machine by an identical motor. For reasons of easier flux measure-

ment by the probe coils and also for the attainment of the air-gap distribution, the rotor of the test machine was mechanically blocked to prevent rotation in either direction. The block was accomplished by fastening ends of two steel plates to the coupling between the two dc machines so that the rotary motion was retarded by the pressure of the ends of these arms against the bedplate.

With the rotor blocked, armature short circuit was simulated by impressing a step voltage to the armature circuit winding for several winding connections under different degrees of initial saturation provided by the shunt field excitation. The magnitude of the step voltage was varied by using different series combinations of a 30-volt 1390-ampere dc generator and a 32-volt battery composed of the submarine Type Sargo cells.

Bar-To-Bar Voltage Measurements

For reasons of simplicity and due to oscillograph limitations, it was necessary to obtain the bar-to-bar voltages between alternate bars on the main commutator by means of an auxiliary commutator with half the total number of segments (Figure A3). Spring strips of phosphor bronze with silvered contact surfaces are employed to pick off the voltages from the auxiliary commutator. These strips were locked in place by wooden plugs in the auxiliary brush holder. By shaping the ends of the strips, it was possible to locate them accurately with respect to the commutator bars. It is important that a high impedance metering system be employed to measure these bar-to-bar voltages in order to eliminate any further voltage drops.

iii

(1) 2600-ampere circuit breaker
(2) 90-hp dc controller
(3) 90-hp drive motor
(4) 90-hp test machine
(5) 3000-ampere short-circuit switch
(6) Interpole winding
(7) Series field winding
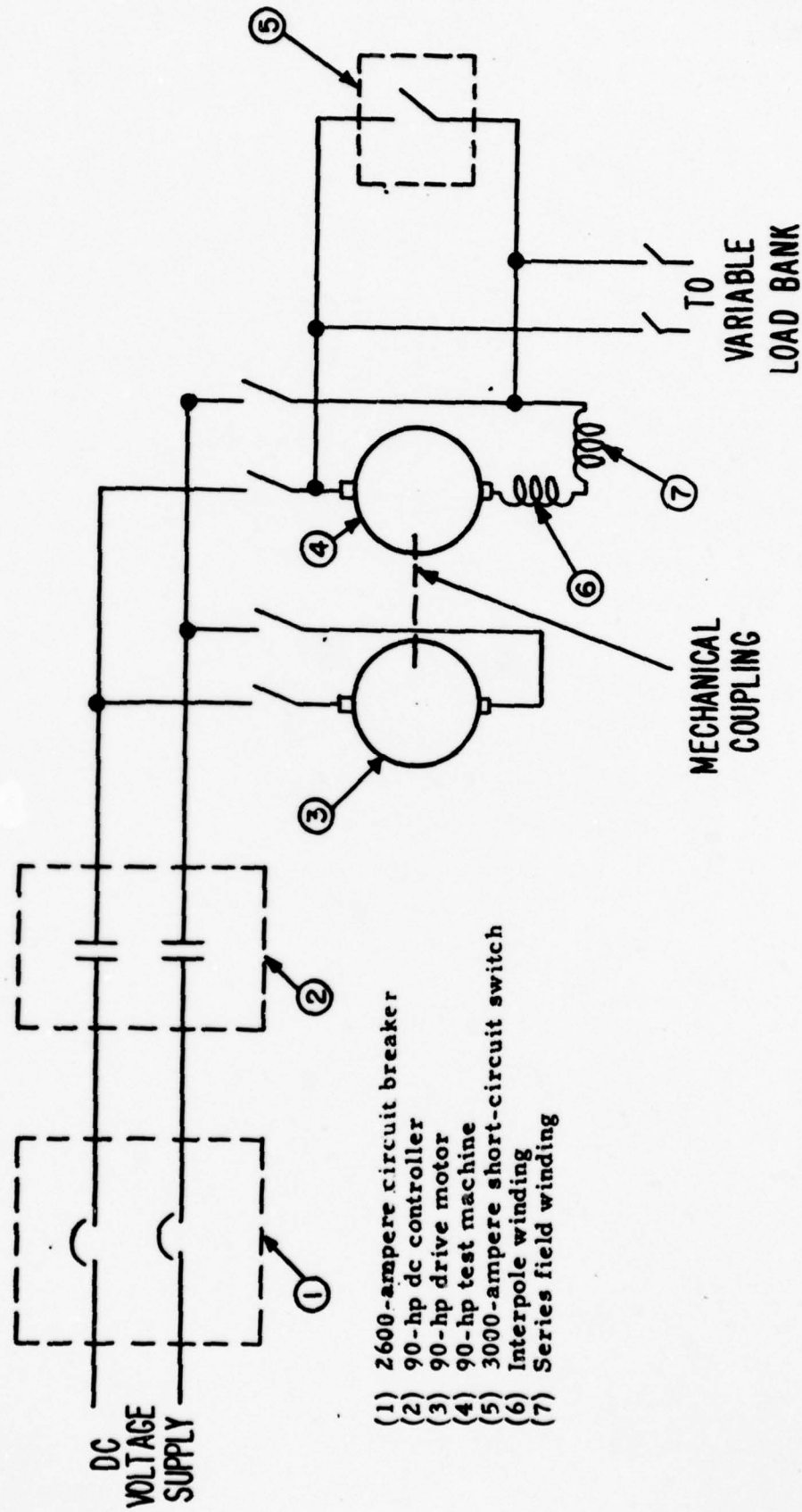
Figure A1 - Schematic diagram of 90-hp dc test machine

Note: (a) Each probe coil consists of 5 turns of #26 Formex insulated wire.
(b) Connections to each coil are brought outside
(c) when

Main pole core
Main pole shoe
Interpole core   } is measured all
Interpole shoe
applicable coils are connected in series making a total of 20 turns.

INTERPOLE CORE
PROBE COIL

MAIN POLE CORE
PROBE COIL

MAIN POLE SHOE
PROBE COIL ALSO
LOCATION OF
INTERPOLE SHOE
PROBE COIL
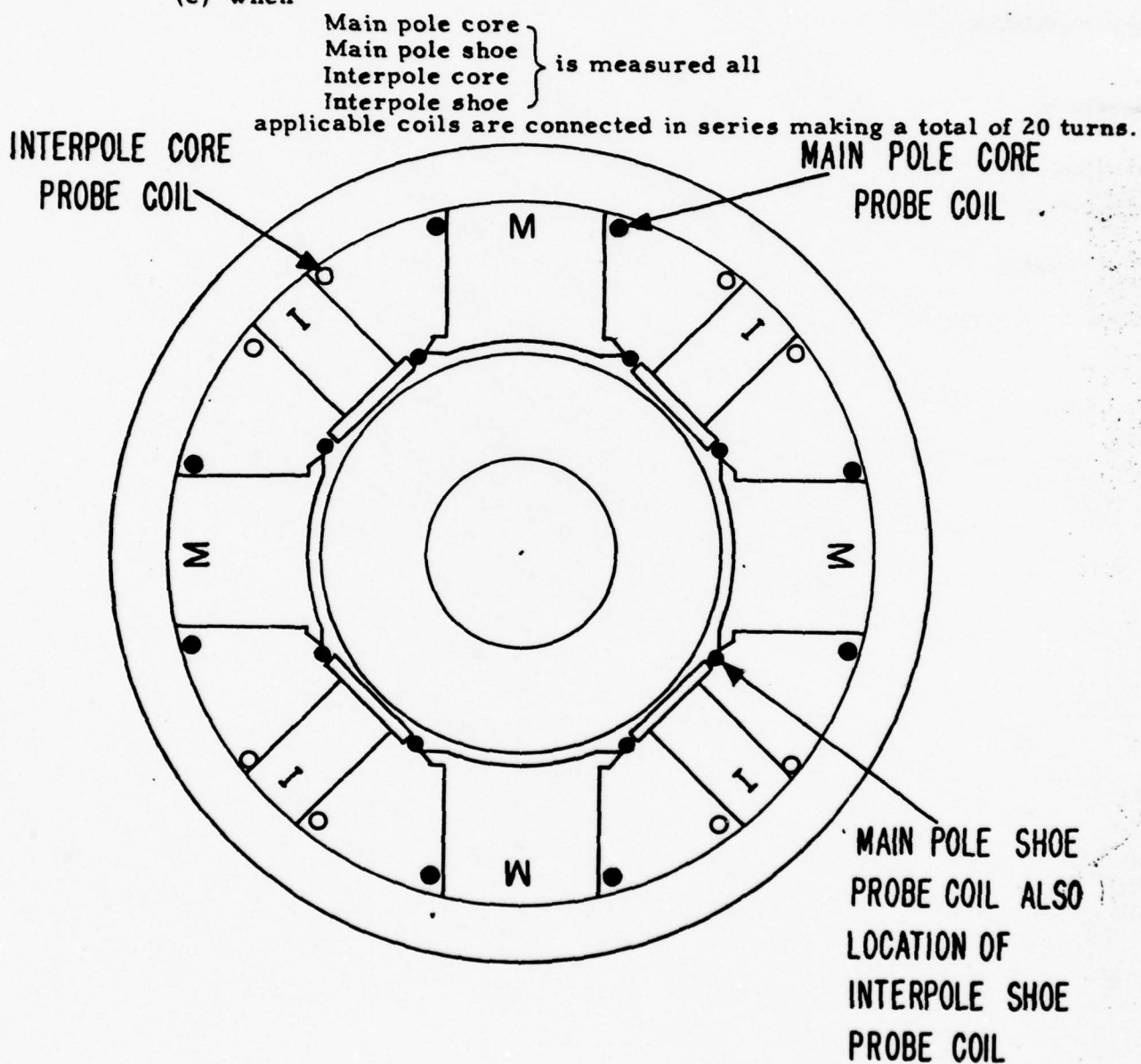
Figure A2 - Location of flux probe coils in 90-hp dc test machine.

ARMATURE

AUXILIARY BRUSH HOLDER

SPRING STRIP
COMMUTATOR

AUXILIARY COMMUTATOR

CURRENT LIMITING
RESISTORS 1500 OHMS

(a)

(b)

SHIELDED
LEADS

AUX. COMMUTATOR
1
2
3
4
5
6

BB1

BB2

BB3

CATHODE FOLLOWERS
EMPLOYED AS VOLTAGE
DETECTORS OFFERING
HIGH IMPEDANCE

BB1

BB2

BB3

CEC
MAG
GALVAN.
OSC.

(c)
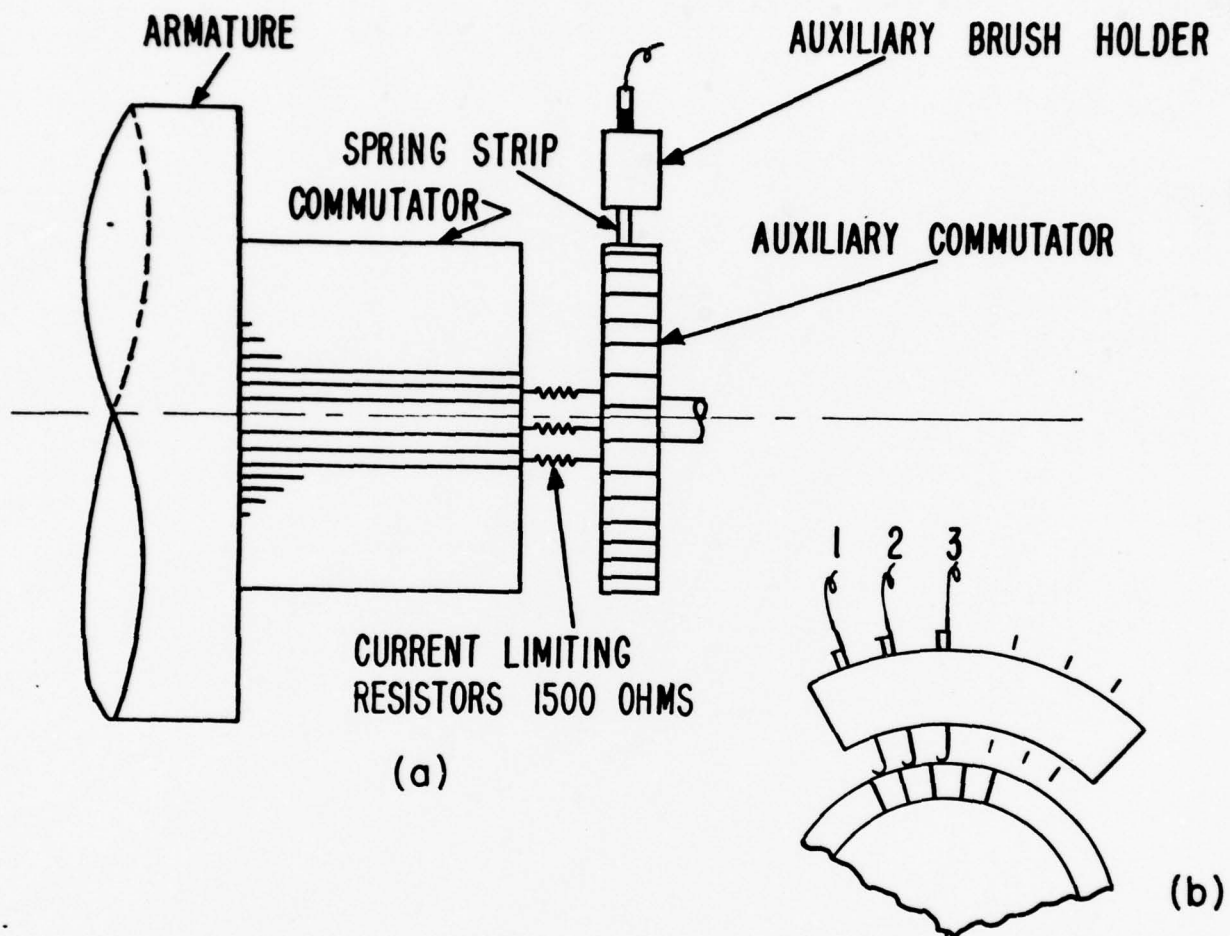
(a) Layout-resistors and auxiliary commutator   (b) Auxiliary brush holder
(c) Schematic diagram

Figure A3 - Bar-to-bar voltage measurement.

ILLUSTRATIONS

FOR

NRL MEMORANDUM REPORT NO. 63

(a) Differential series field connection
(b) Shunt Connection
(c) Cumulative series field connection
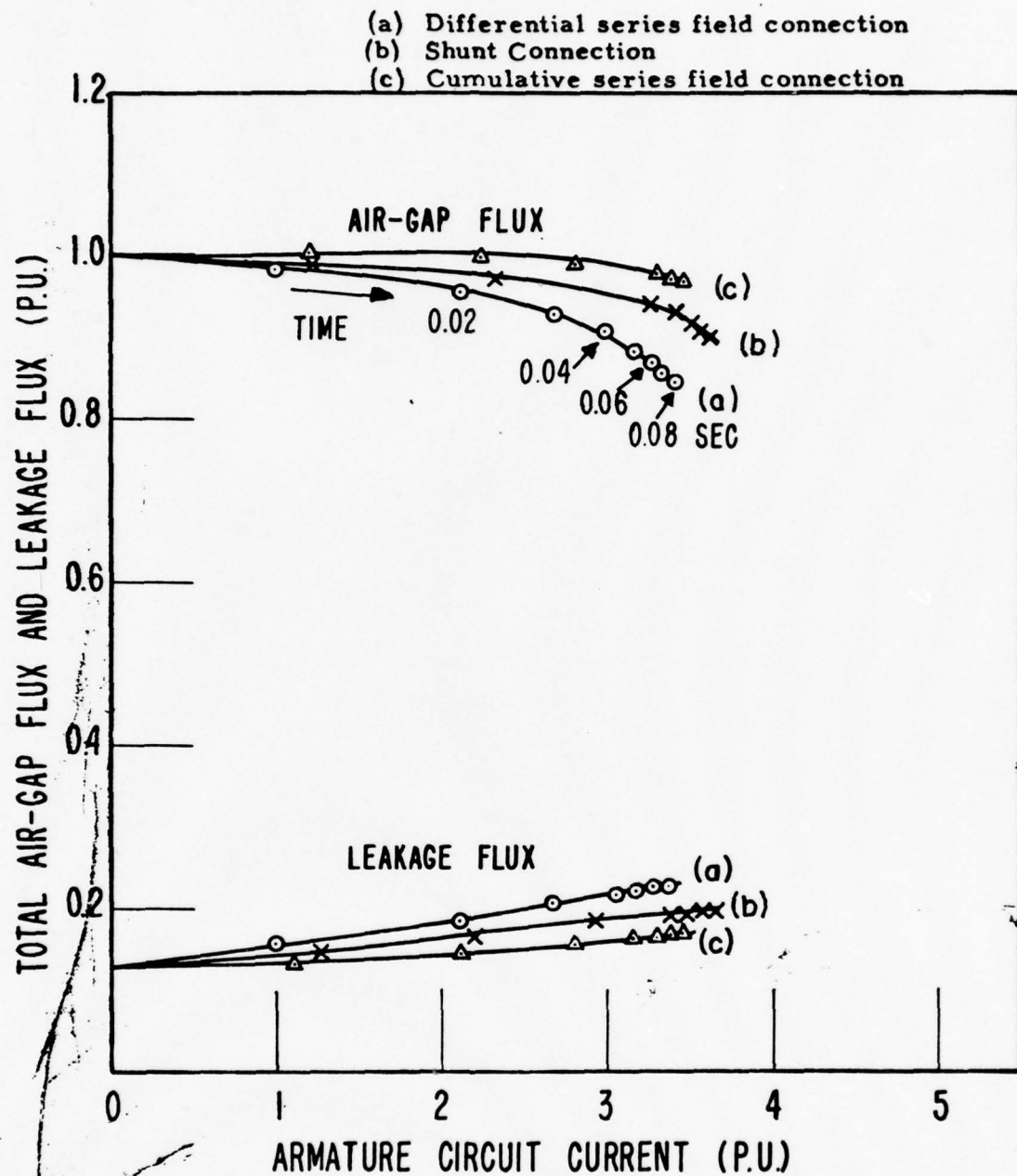
Figure 1 - Relation of air-gap flux to transient armature current. Conditions: machine, in blocked rotor for two degrees of compounding; time, a variable along the curves.
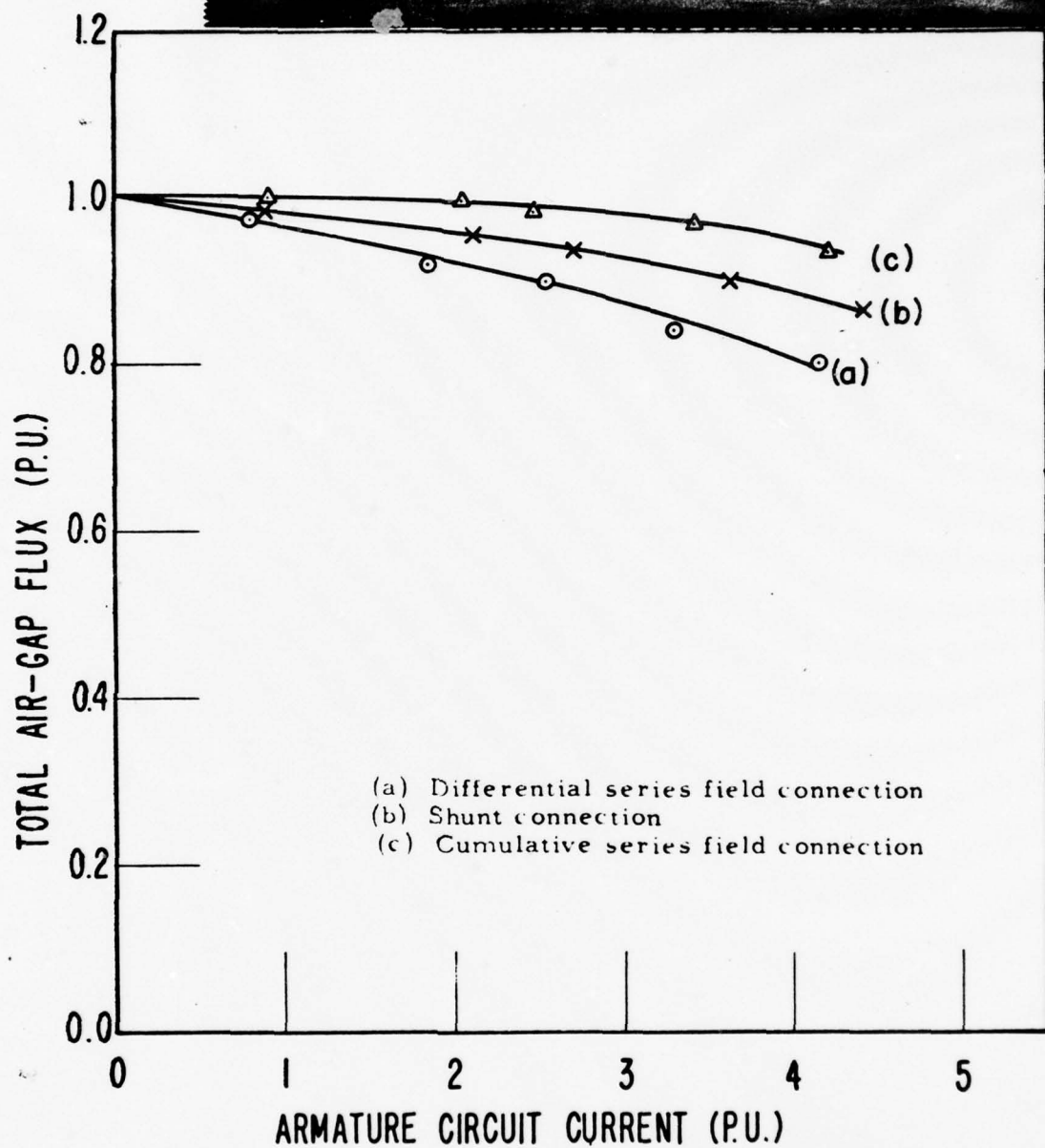
Figure 2 - Relation of air-gap flux to transient armature current. Conditions: machine, in blocked rotor for two degrees of compounding; time, 0.08 second after transient initiation.
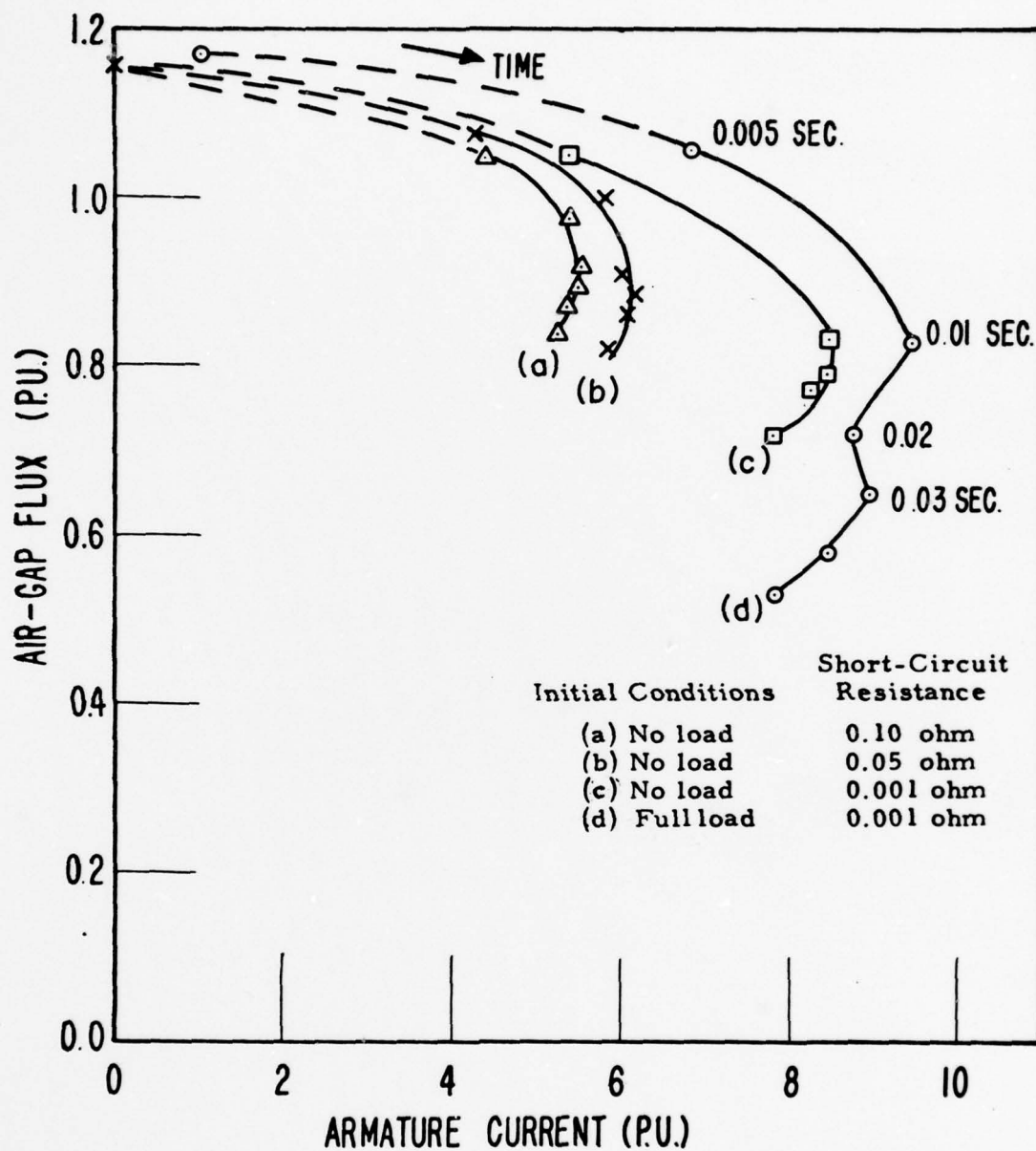
Figure 3 - Relation of air-gap flux during short-circuit tests to transient armature current. Conditions: differential series field connection; time, a variable along the curves.
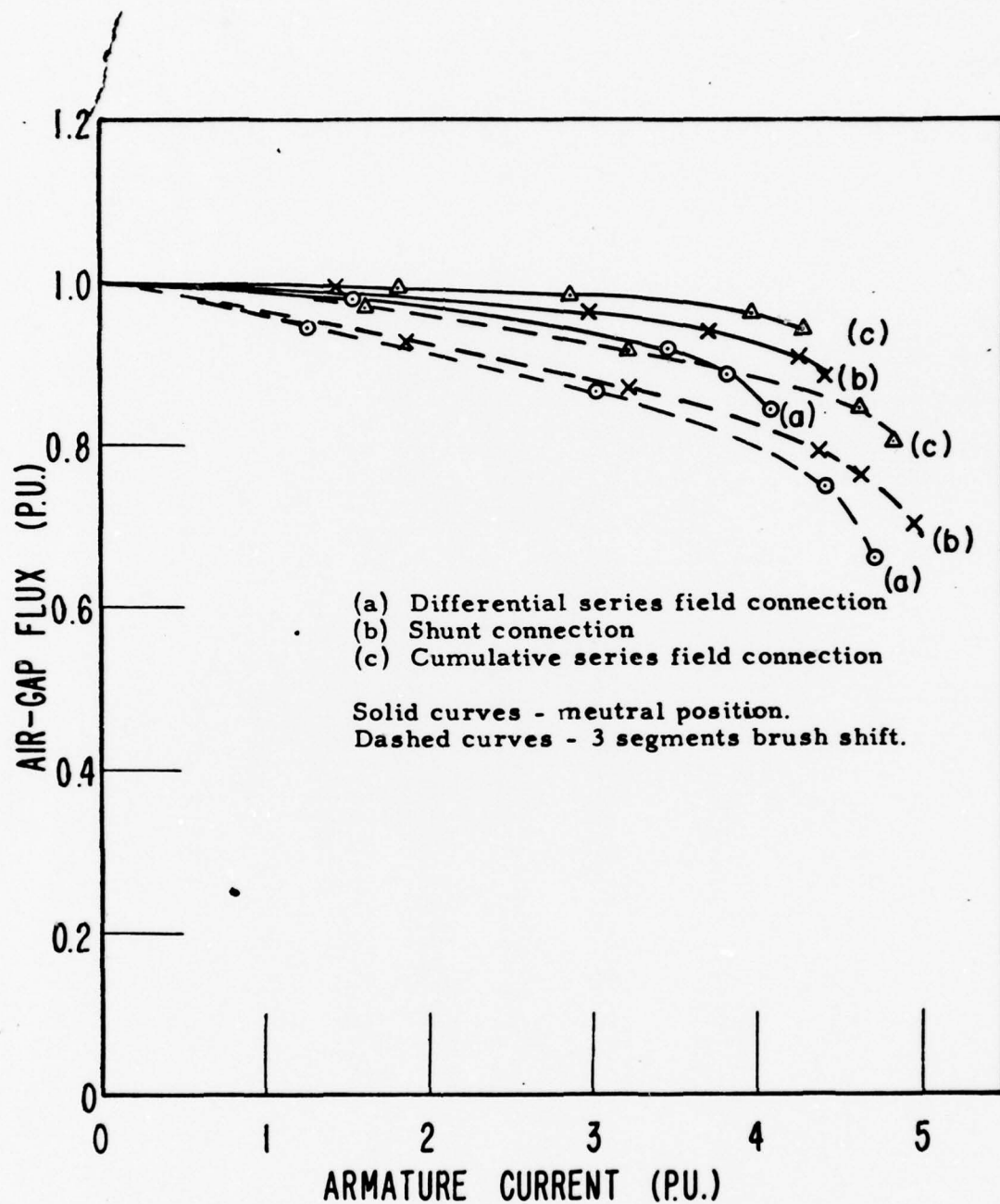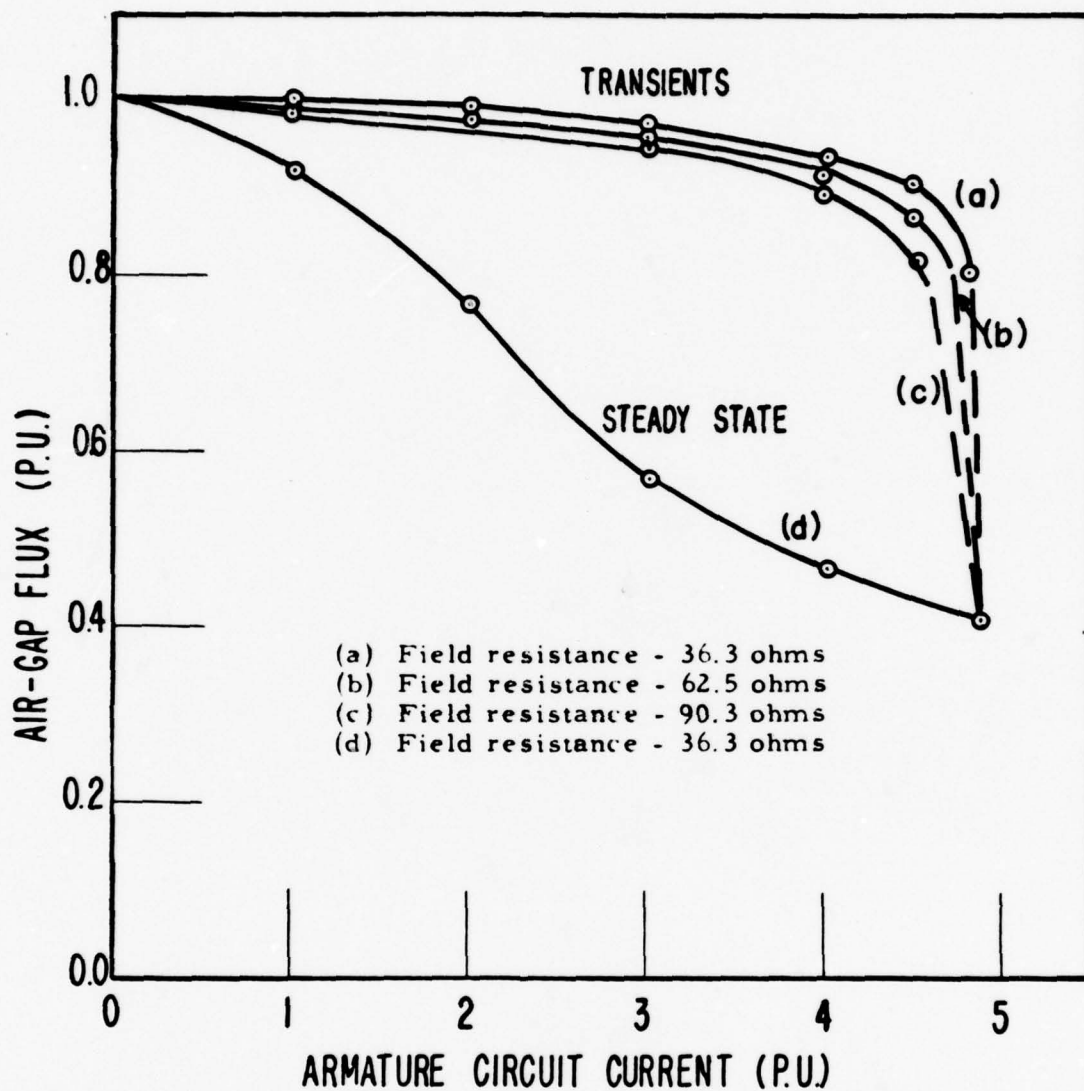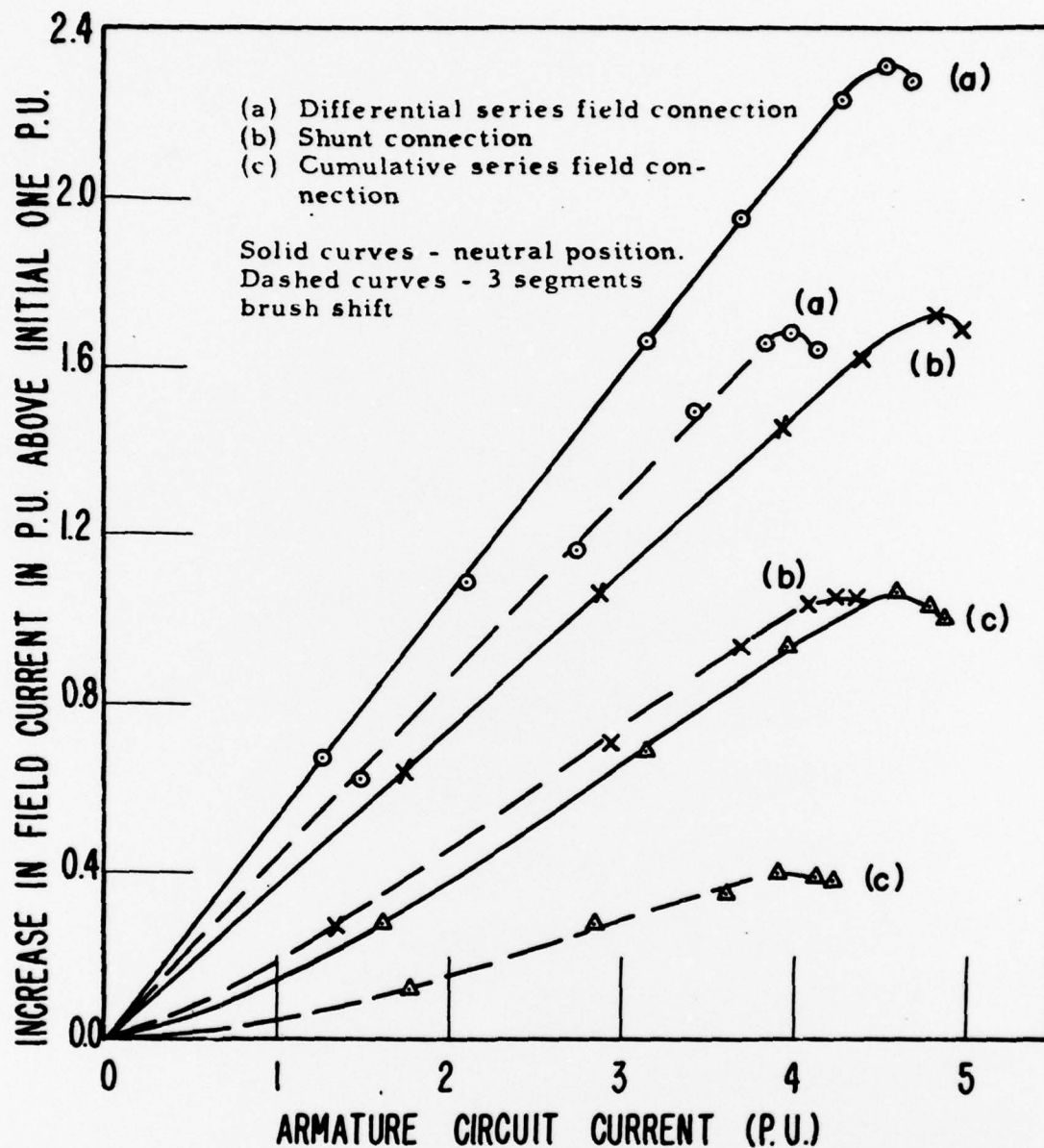
Figure 4 - Effect of brush shift upon the relation of air-gap flux to transient armature current. Conditions: machine, in blocked rotor for two degrees of compounding; time, a variable along the curves.
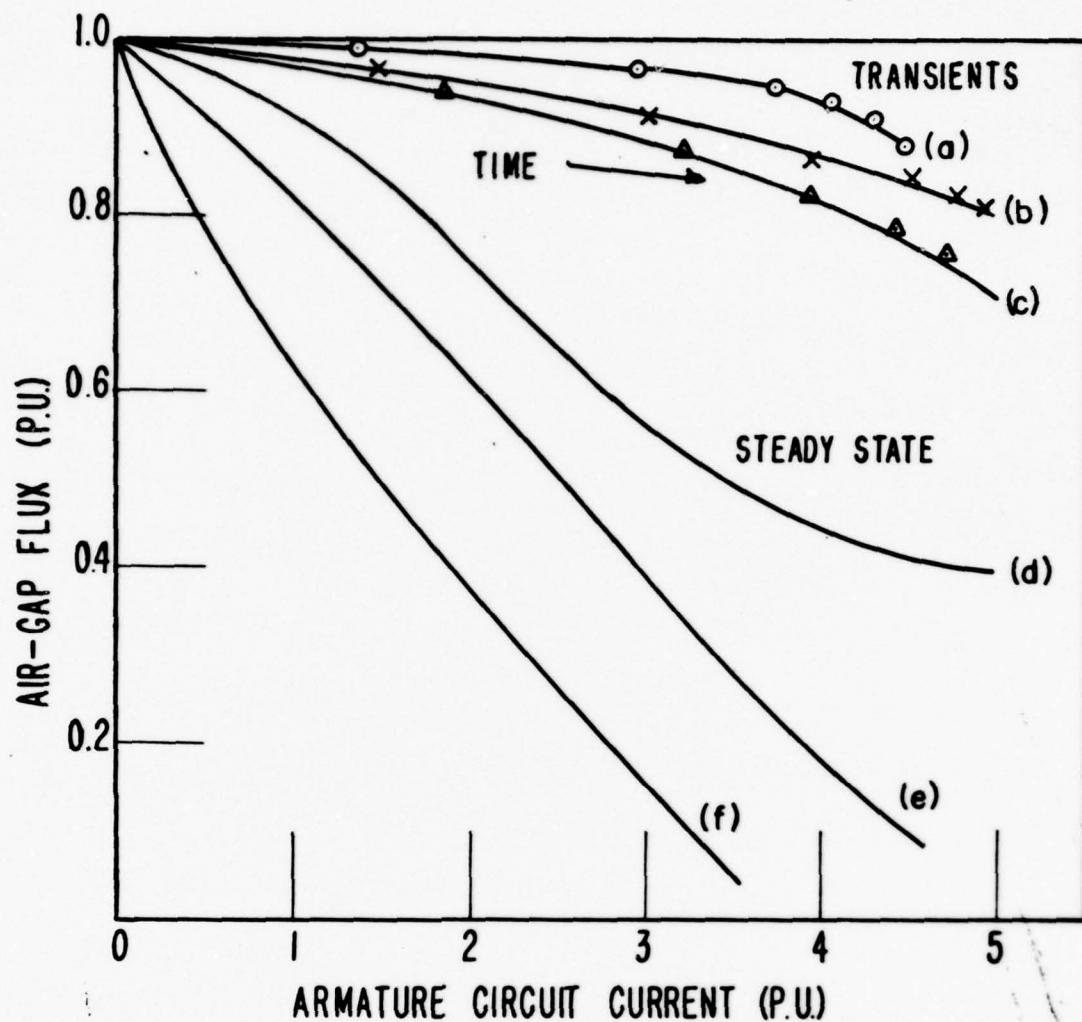
Transient current: time, a variable along the curves

(a) Neutral position of the brushes
(b) Three additional shorted commutator segments in direction of rotation
(c) Three-segment brush shift in direction of rotation

Steady-State Current

(d) Neutral position of the brushes
(e) Three additional shorted commutator segments in the direction of rotation
(f) Three-segment brush shift in direction of rotation.

Figure 5 - Comparison of the effects of brush width and brush shift upon the relation of air-gap flux to transient and steady-state armature current. Condition: machine, in blocked rotor for shunt connection.
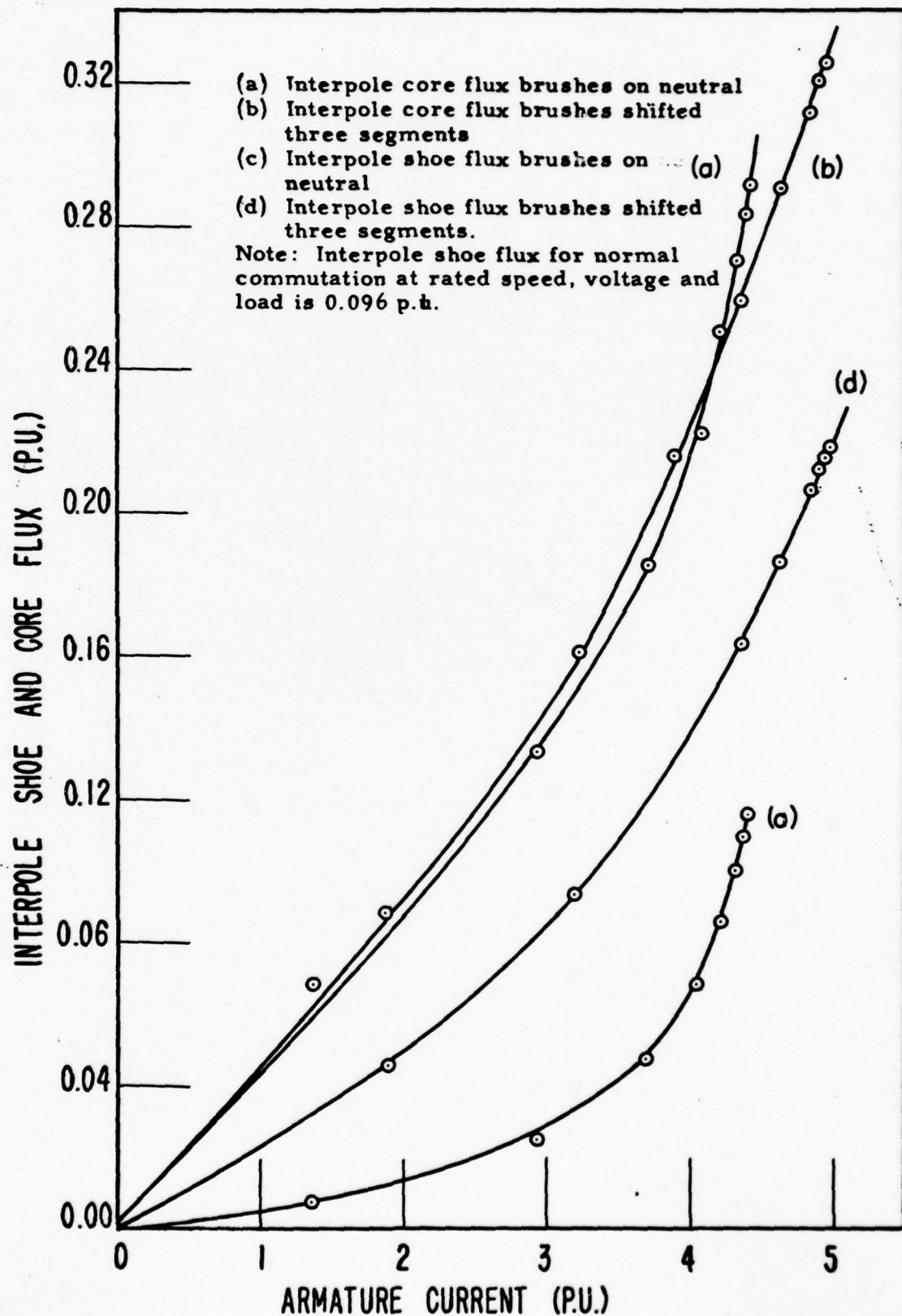
Figure 6 - Effect of brush shift on the build-up of interpole shoe and core flux in relation to transient armature current. Conditions: machine, in blocked rotor for shunt connection: time, a variable along the curves.

Figure 7 - Relation of interpole shoe and core flux during short-circuit tests to transient armature current. Conditions: differential series field connection: time, a variable along the curves.

Solid curves - interpole core. Dashed curves - interpole shoe
Note: Interpole shoe flux for normal commutation at rated speed, voltage and load is 0.096 p.u.

(a) No Load Initially   0.10 ohm Short-Circuit Resistance
(b) No Load Initially   0.05 ohm Short-Circuit Resistance
(c) No Load Initially   0.001 ohm Short-Circuit Resistance
(d) Full Load Initially   0.001 ohm Short-Circuit Resistance

Figure 8 - Relation of shunt pole leakage flux during short-circuit tests to transient shunt field current. Conditions: Differential series field connections; time, a variable along the curves.

Figure 9 - Relation of transient and steady-state air-gap flux to armature current for different resistances in the shunt field circuit. Condition: machine in blocked rotor for shunt connection.
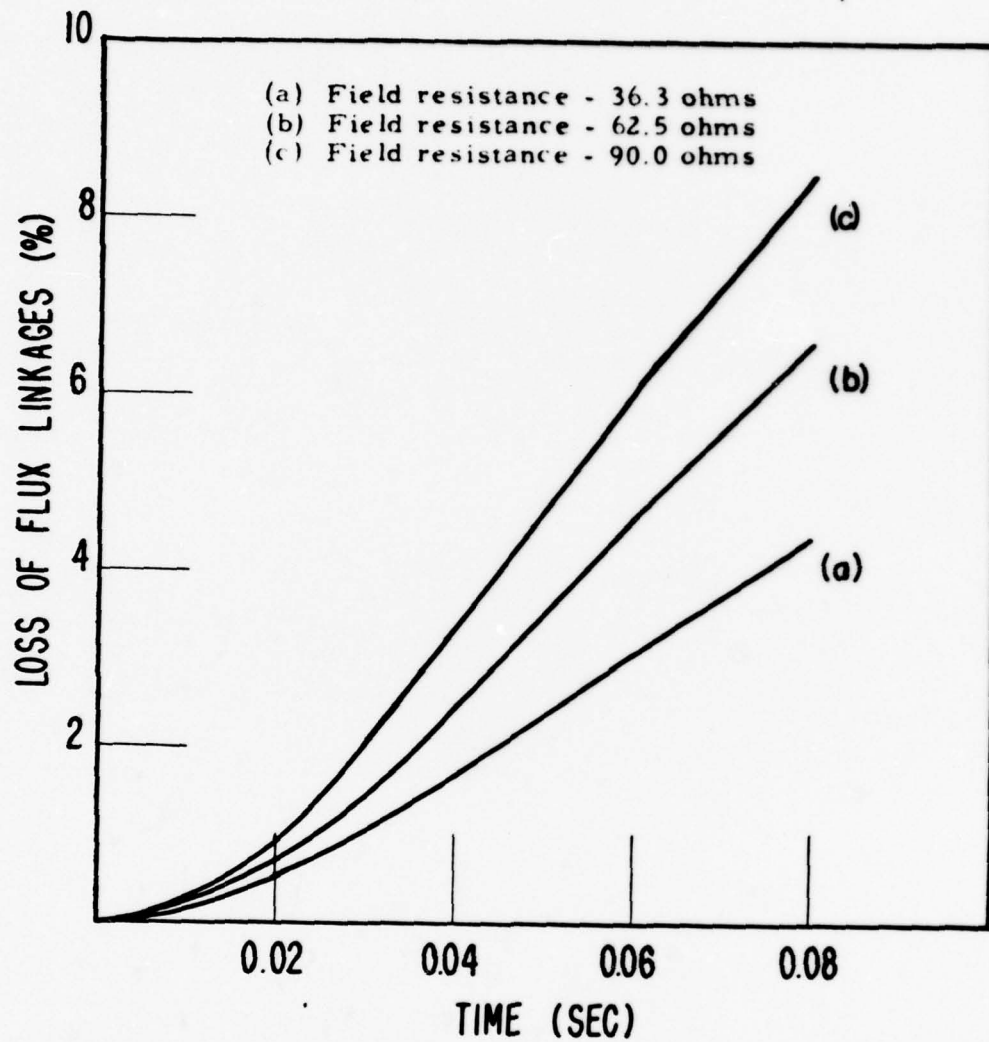
Figure 10 - Loss of flux linkages for different resistances in the shunt field circuit as a function of time (expressed as a percentage of the initial linkages). Condition: machine in blocked rotor for shunt connection.
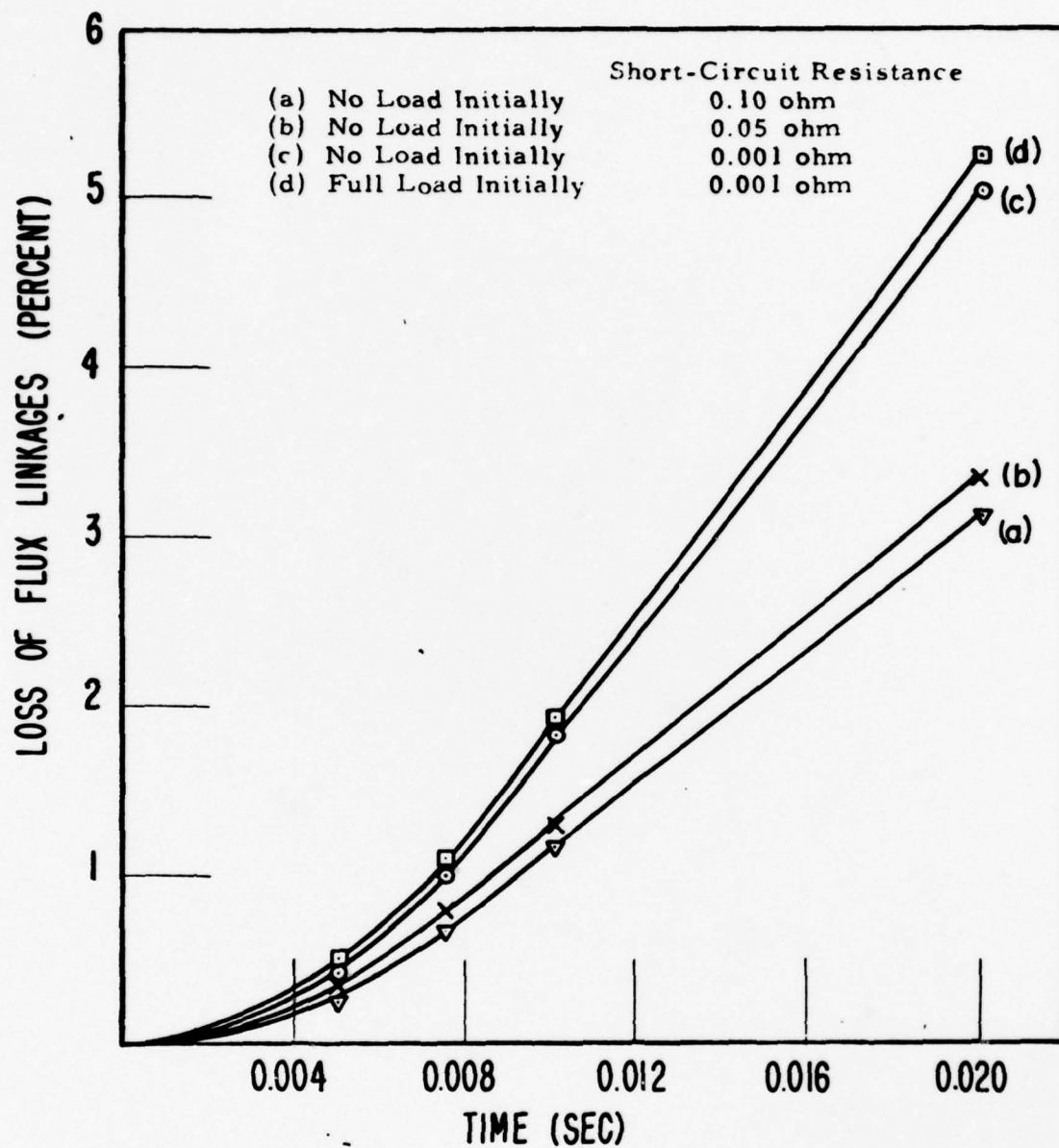
Figure 11 - Loss of flux linkages during short-circuit tests as a function of time. Condition: differential series field connection.

Figure 12 - Effect of brush shift on the relation of incremental shunt field current to transient armature current. Conditions: machine in blocked rotor for two degrees of compounding; time, a variable along the curves.
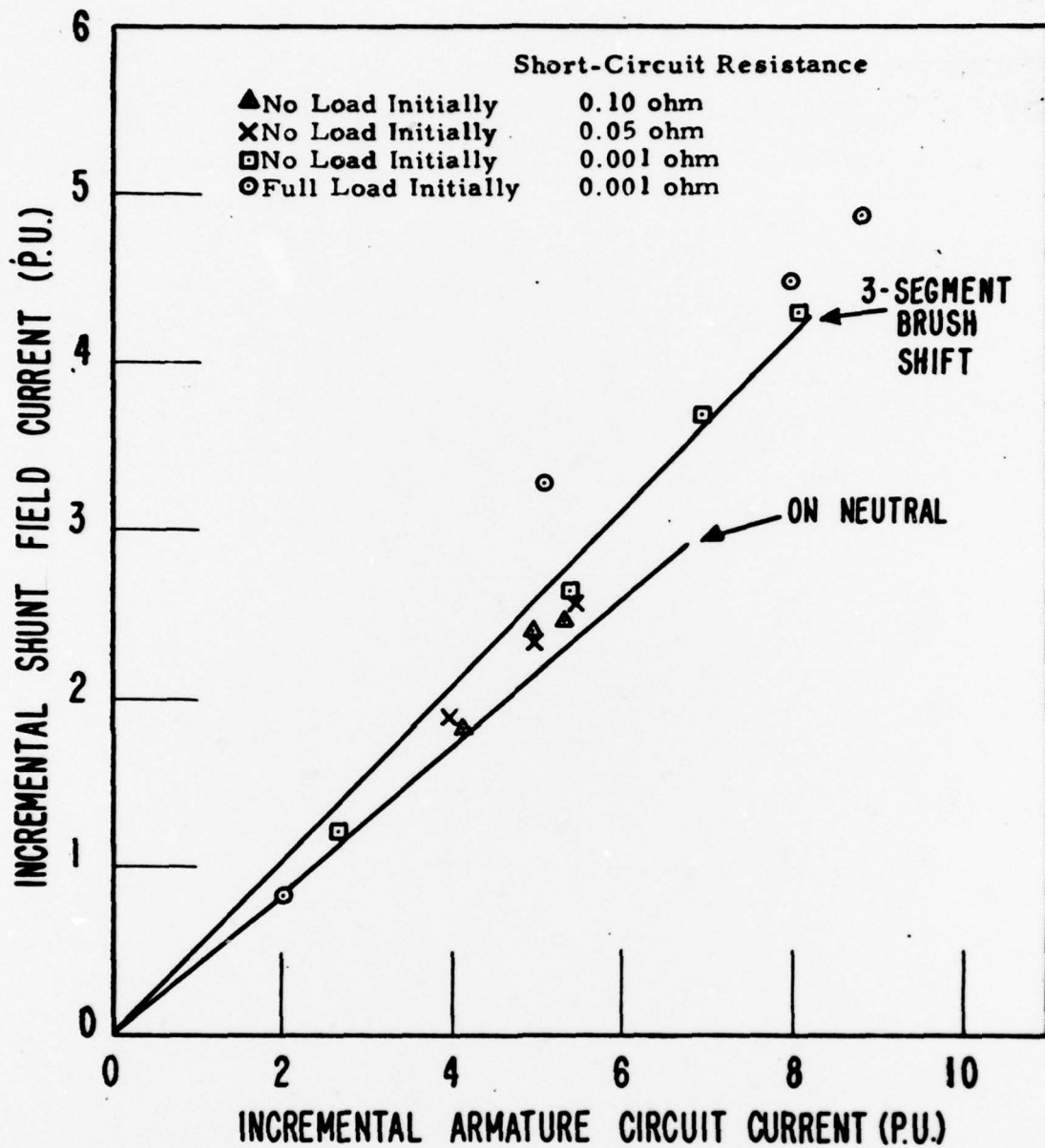
Figure 13 - Comparison between blocked rotor and short-circuit tests as regards the relation of incremental shunt field current to transient armature current. Conditions: differential series field connection; time, a variable along the curves.
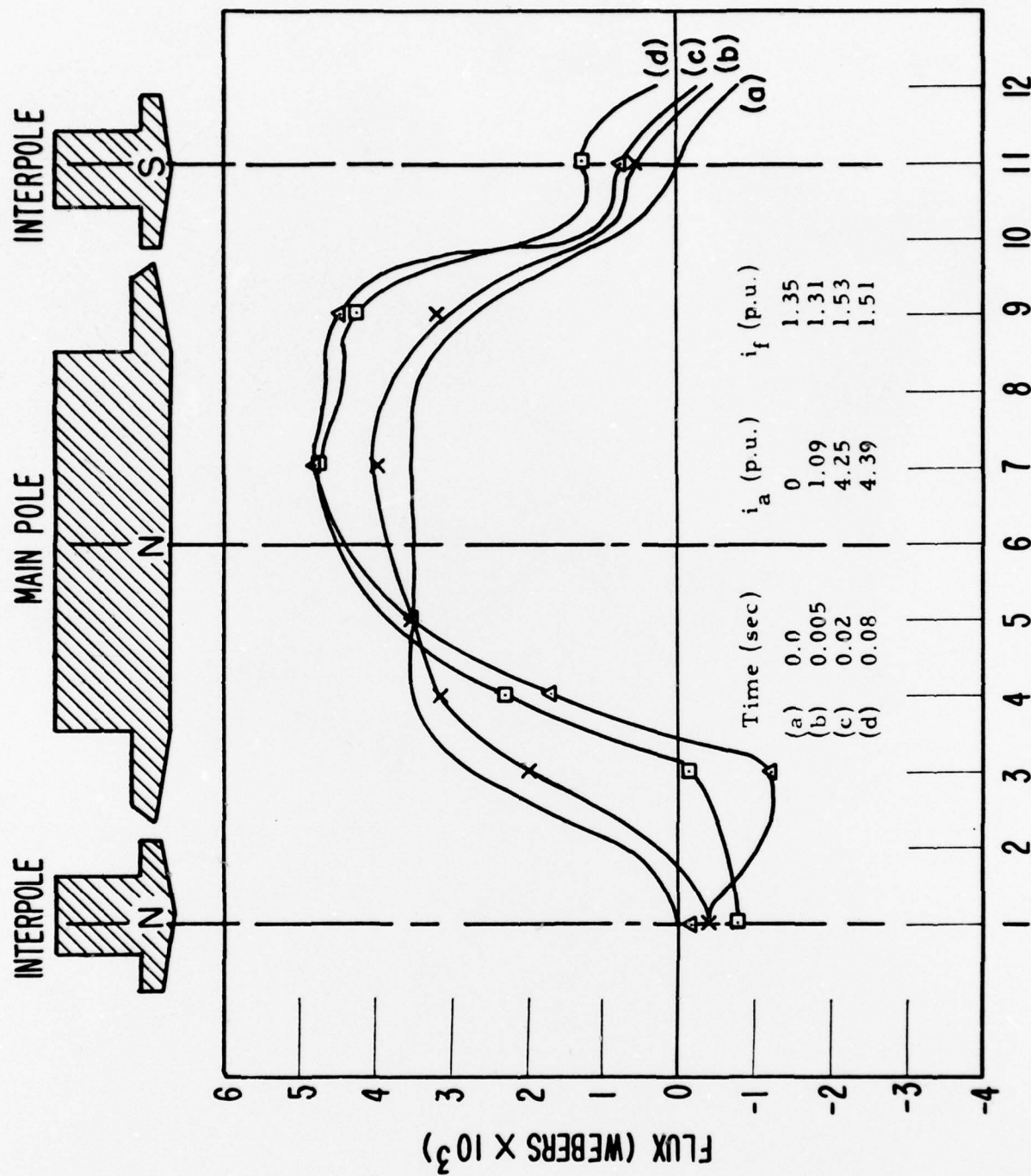
COIL NUMBER AND LOCATION WITH RESPECT TO POLE STRUCTURES
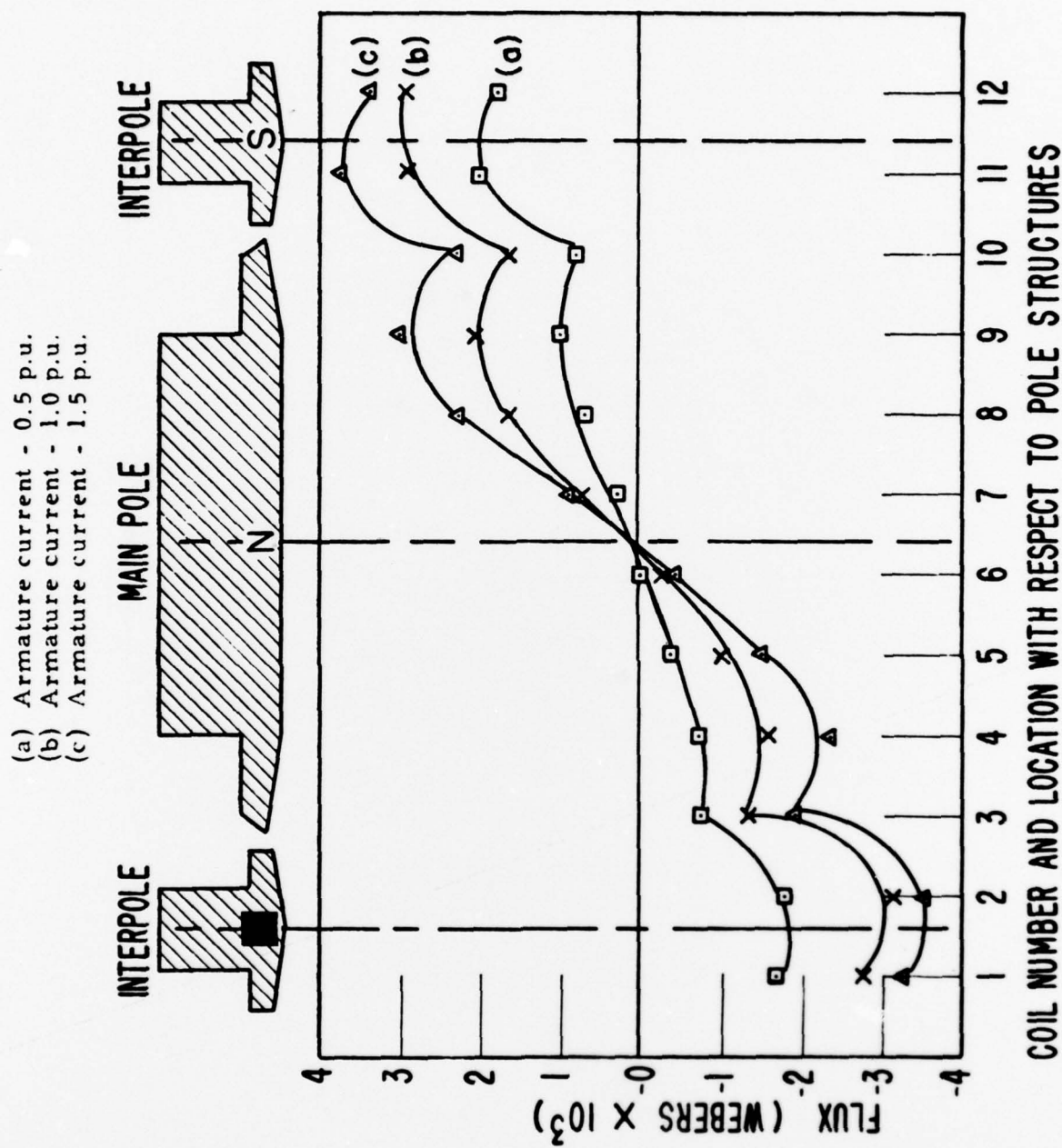
Figure 14 - Steady-state air-gap flux change as a function of armature current. Conditions: machine in blocked rotor: no shunt field excitation: interpole winding disconnected.

Figure 15 - Steady-state air-gap flux change as a function of armature current. Conditions: machine in blocked rotor; shunt field excitation 1.5 p.u.; no interpole excitation.

Figure 16 - Steady-state air-gap flux distribution as a function of armature current. Conditions: machine in blocked rotor; shunt field excitation 1.5 p.u.; interpole winding disconnected.

(a) Initial distribution - 1.5 p.u. shunt field excitation

(b) Armature current - 0.5 p.u.

(c) Armature current - 1.0 p.u.

(d) Armature current - 1.5 p.u.

INTERPOLE　　MAIN POLE　　INTERPOLE

S　　N　　N

Time (sec)	i_a (p.u.)	i_f (p.u.)
(a)	0.0	0	1.35
(b)	0.005	0.94	1.74
(c)	0.02	2.76	2.59
(d)	0.08	4.32	2.73

(d)
(c)
(b)
(a)

1　2　3　4　5　6　7　8　9　10　11　12

COIL NUMBER AND LOCATION WITH RESPECT TO POLE STRUCTURES

6　5　4　3　2　1　0　-1　-2　-3　-4

FLUX (WEBERS X 10³)

Figure 17 - Transient air-gap flux distribution. Conditions: machine in blocked rotor; cumulative series field connection; interpole winding connected.

Figure 19 - Transient air-gap flux distribution. Conditions: machine in blocked rotor; cumulative series field connection; interpole winding connected.
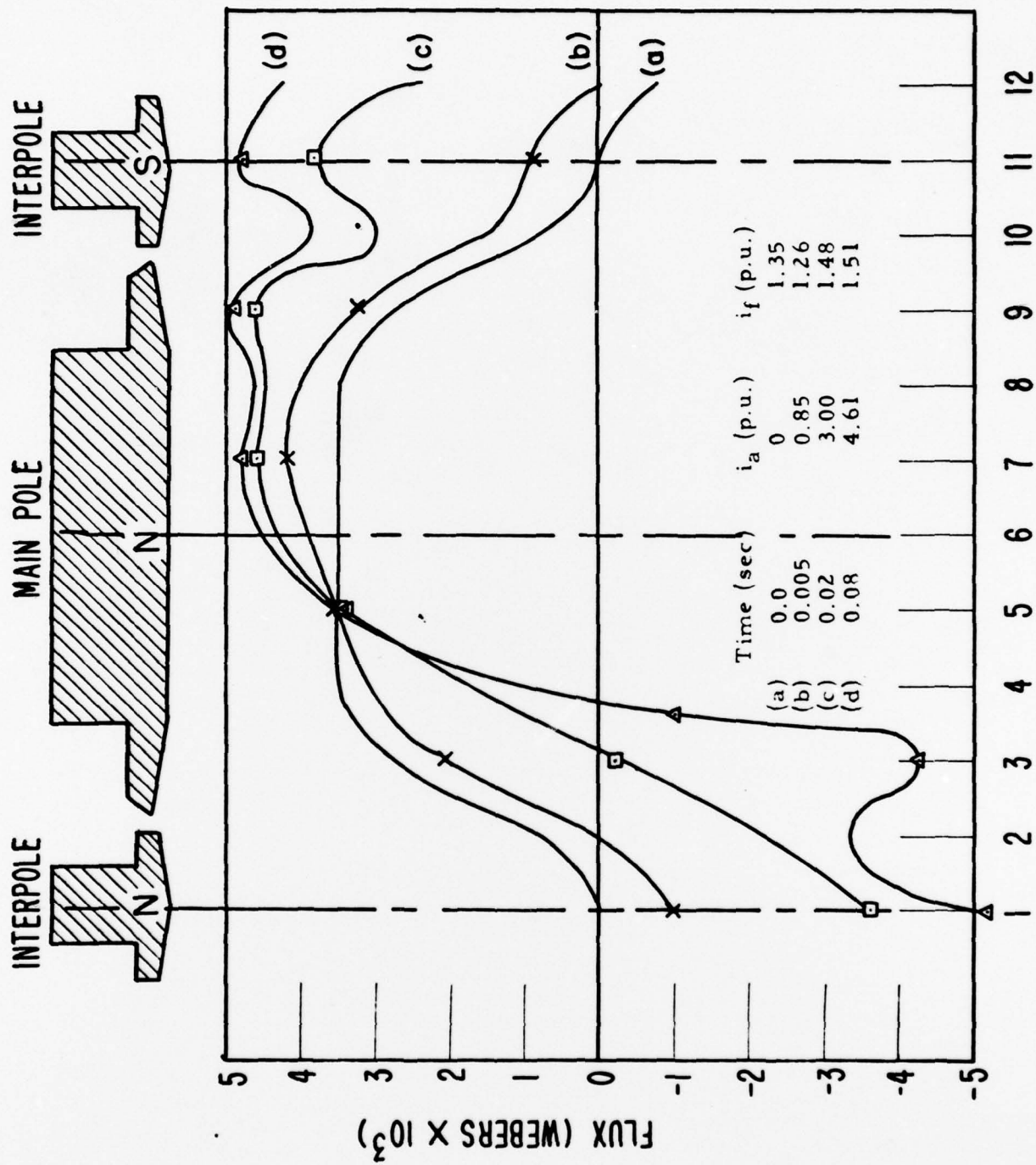
Figure 20 – Transient air-gap flux distribution. Conditions: machine in blocked rotor: cumulative series field connection: interpole winding disconnected.
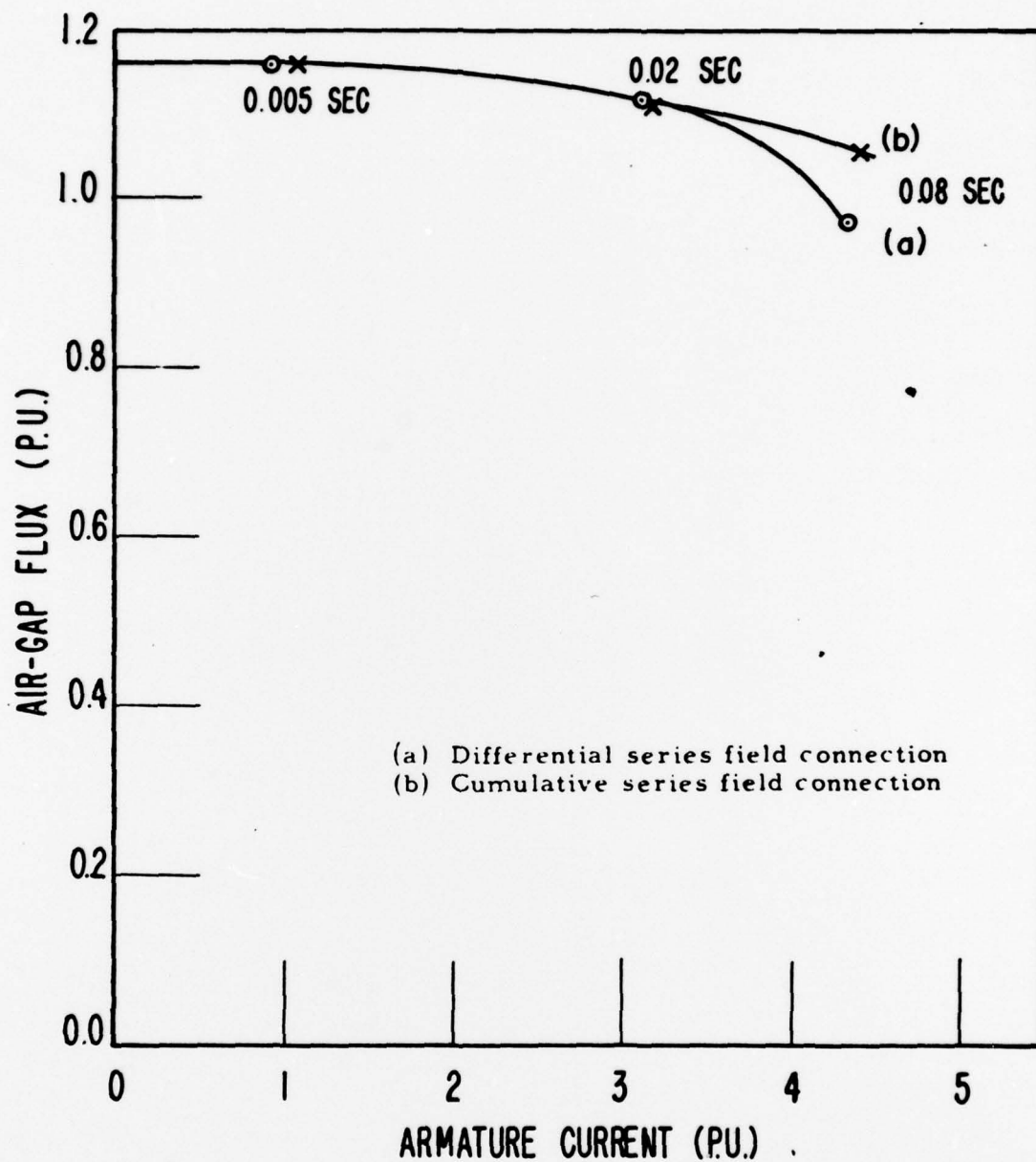
Figure 21 - Relation of total air-gap flux to transient armature current. Obtained from air-gap flux distribution. Conditions: machine in blocked rotor for two degrees of compounding: interpole winding connected: time, a variable along the curves.
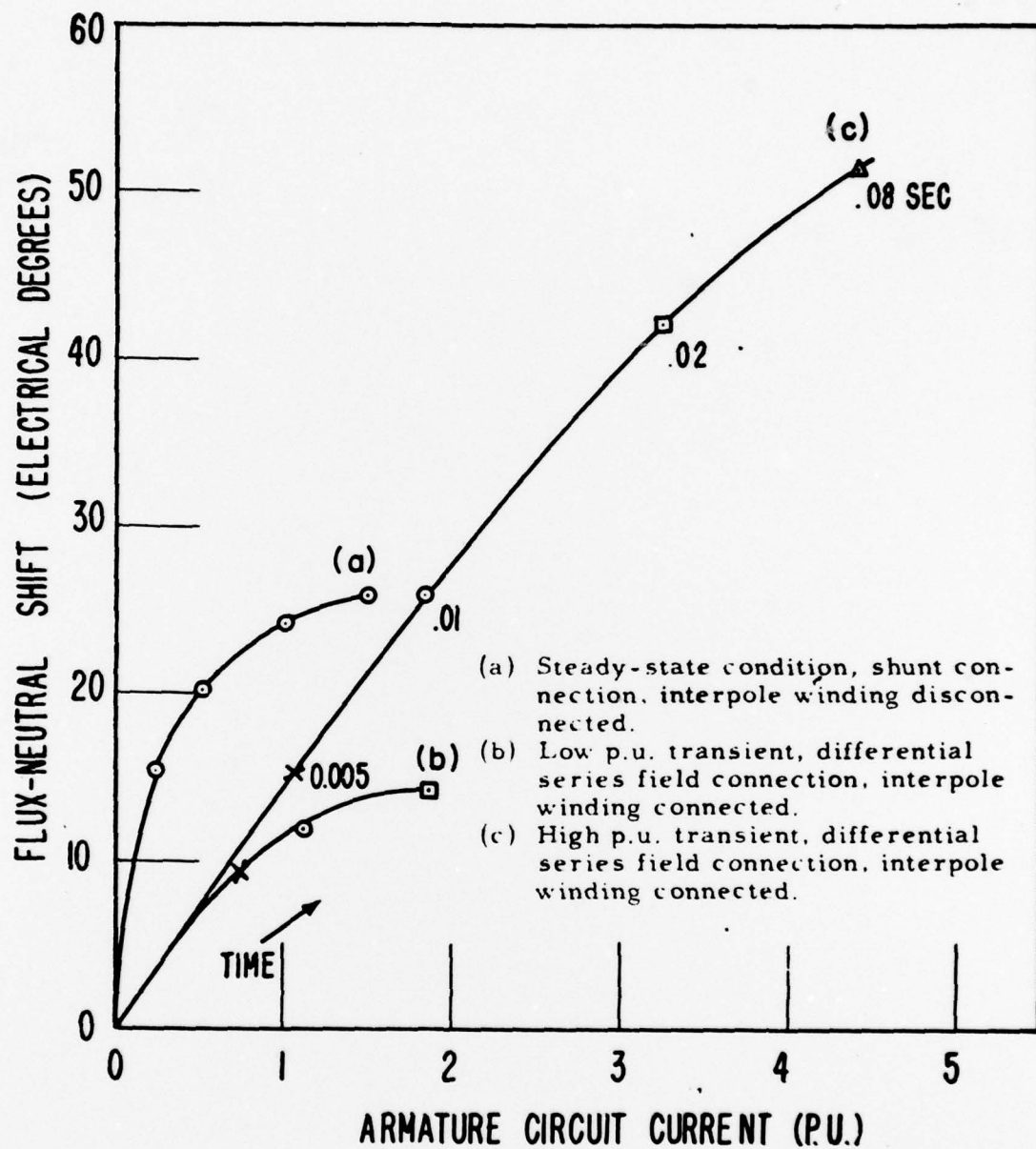
Figure 22 - Relation of flux-neutral shift to armature current in steady-state and transient. Condition: machine in blocked rotor.
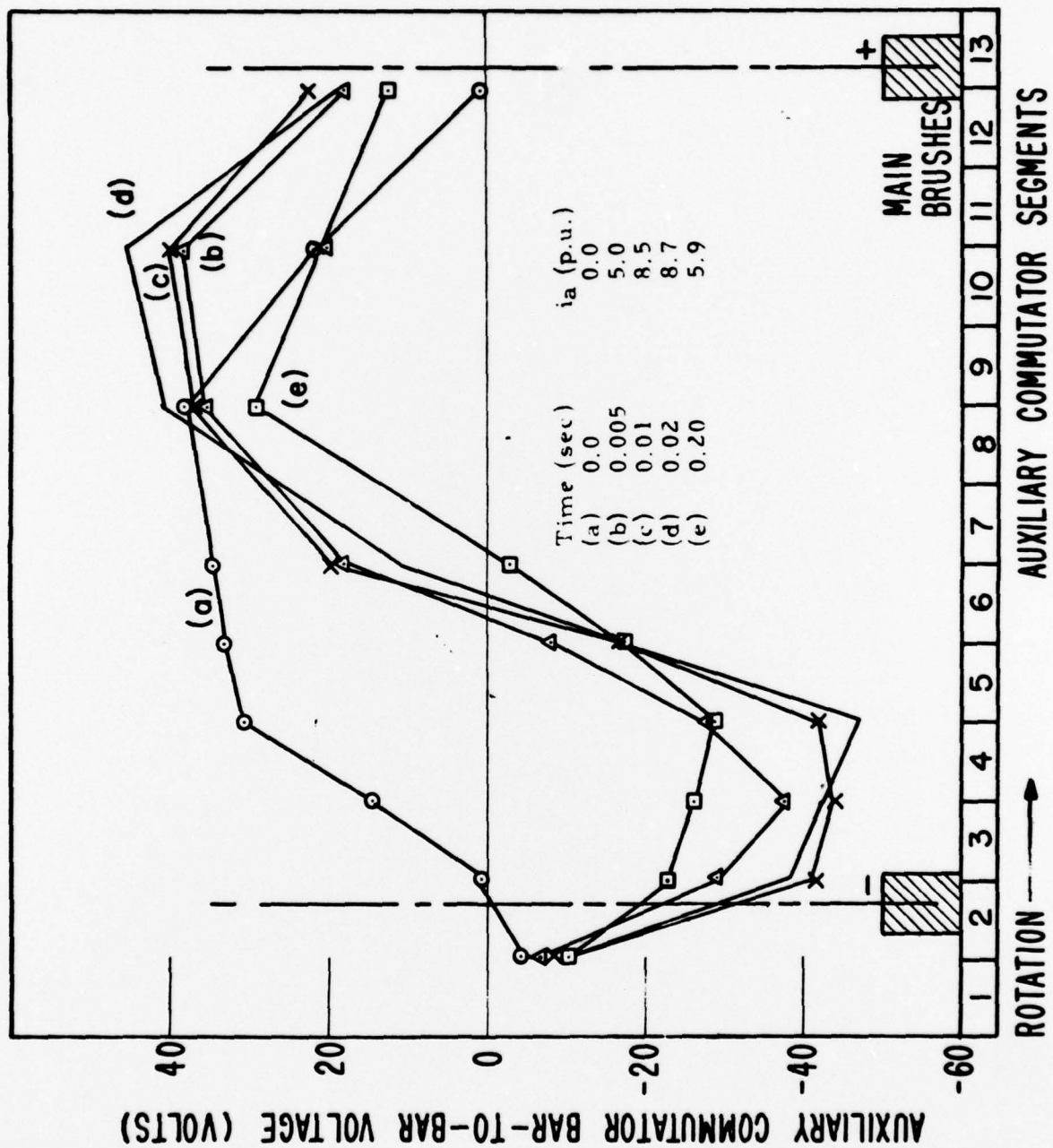
Figure 23 - Bar-to-bar voltage distribution during a short-circuit test.
Initial conditions: no load, 250 volts, 1750 rpm; short-circuit resistance
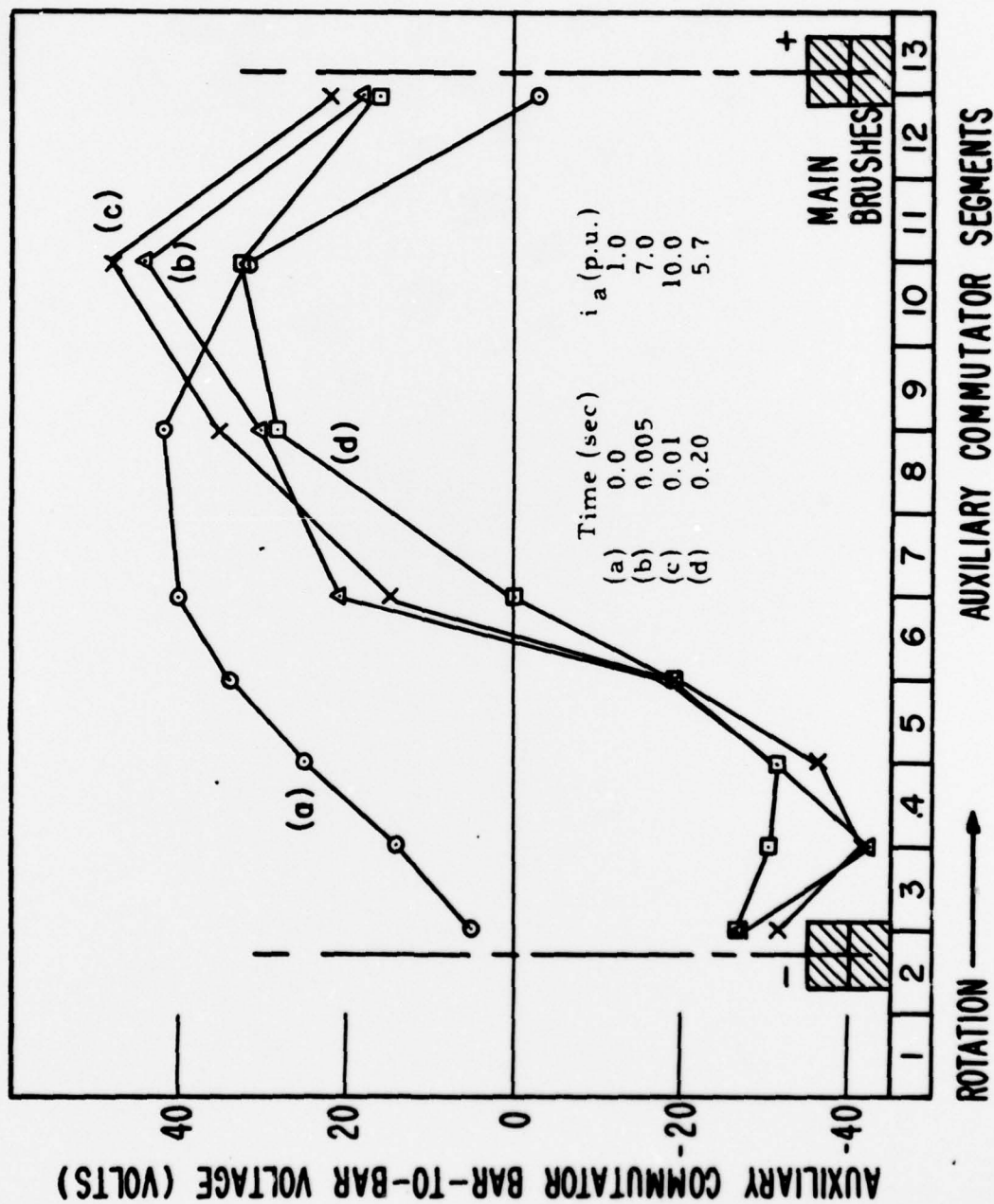0.001 ohm, differential series field connection

Figure 24 - Bar-to-bar voltage distribution during a short-circuit test. Initial conditions: full load, 250 volts, 1750 rpm, short-circuit resistance 0.001 ohm, differential series field connection.
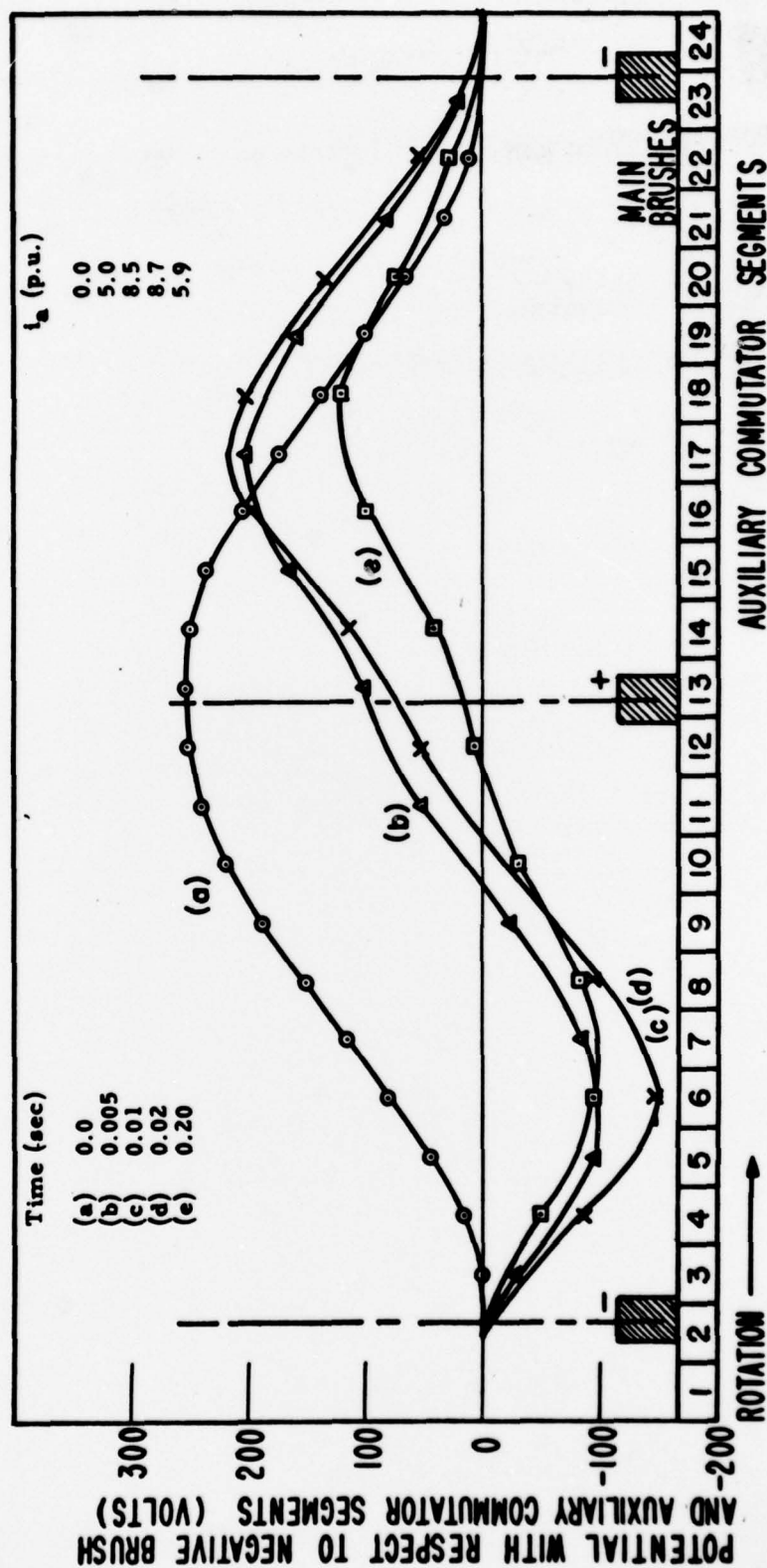
Figure 25 - Voltage distributions during short-circuit tests. Expressed with respect to a negative brush. Initial conditions: no load, 250 volts, 1750 rpm, short-circuit resistance 0.001 ohm, differential series field connection.
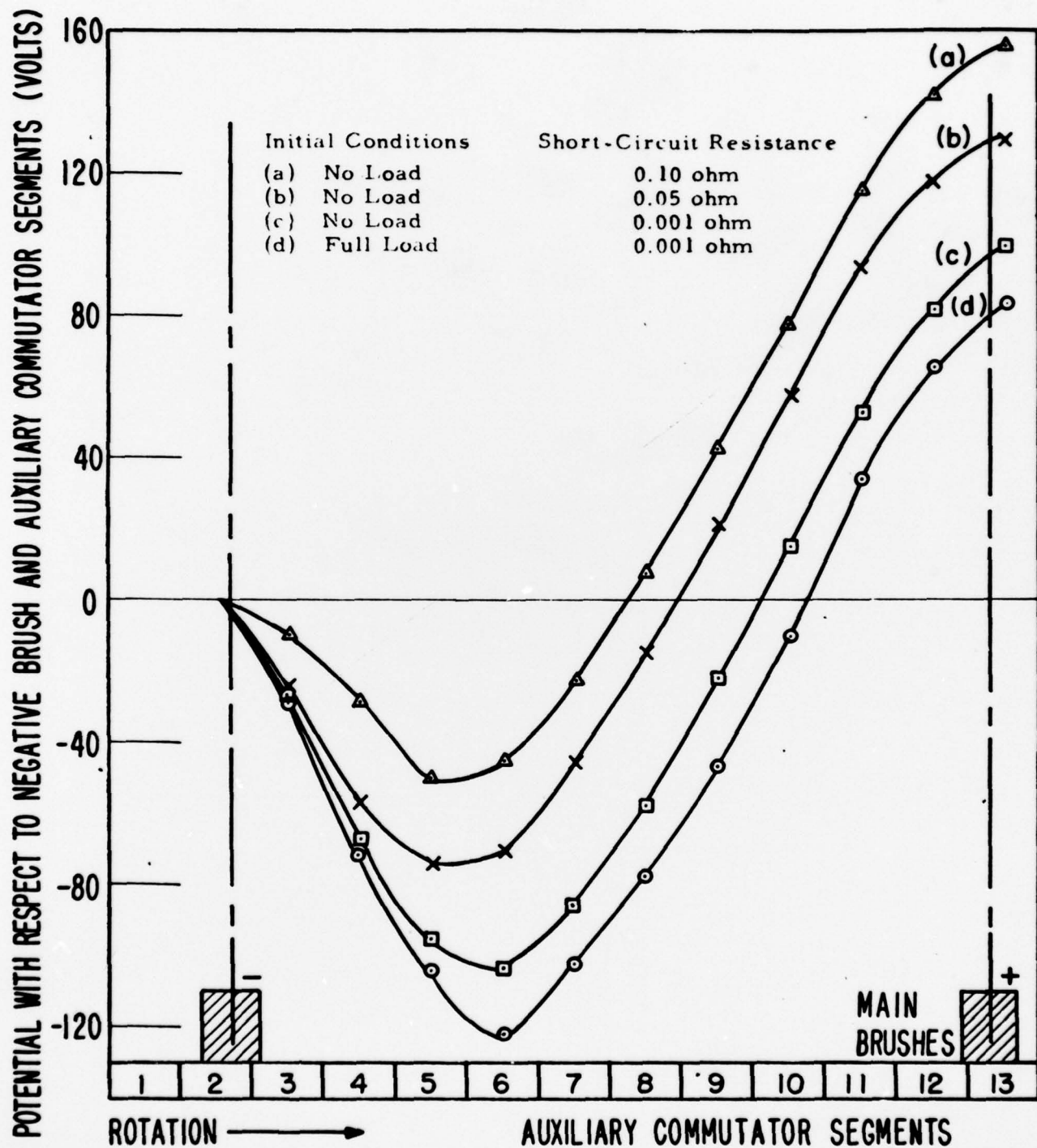
Figure 26 - Voltage distributions during short-circuit tests. Expressed with respect to a negative brush. Initial conditions: 250 volts, 1750 rpm, differential series field connection, time, 0.005 second after short-circuit initiation.